



Swansea University  
Prifysgol Abertawe

# One-Dimensional Modelling of Lung Geometry

Prabhu Muthuganeisan

A thesis submitted in partial fulfillment of the requirements for  
Master of Science in Computational Mechanics

June 2009

Supervisors: Prof. Perumal Nithiarasu and Dr. Raoul van Loon  
School of Engineering, Swansea University

# Abstract

Computational techniques are becoming increasingly valuable in solving and explaining some of the biomedical problems aiding in diagnosis, monitoring and treatment. In this thesis, the usefulness of such modelling techniques to study the airflow through the upper generations of the lower airways in human beings has been highlighted. Unlike the 1-D models for studying blood flows that are common, 1D model of lower airways has remained largely unexplored. The complexity arises from the generation of valid models of lower airways to implementing such models for studying the airflow during various respiratory states. In this study, one-dimensional models of the airways, beginning from Trachea, using the geometric data published by Weibel and Horsfield have been used. The airflow waveform used in this study assumes a realistic pressure waveform corresponding to a peak flow rate of 1.3 l/s and is applied at the inlet of the Trachea. The former model assumes that each parent airway bifurcates into two daughter airways whereas the later model highlights the unsymmetric branching. Locally Conservative Galerkin (LCG) method has been used to solve the set of 1-D equations of the viscous flow. This method has been demonstrated to be effective in solving 1D network models of blood flow [Mynard ] due to its ability to incorporate vessel branching. Some simple problems were used to highlight the ability of the method to handle discontinuities and their influence on the flow. The Weibel models are then implemented to study the airflow through the upper generations of lower airways and the changes to the pressure and velocity due to the branching at each generation are then studied. Some model studies are then presented to study the obstruction identification in the lower airways when some vessels are partially or completely blocked to represent the obstructive diseases occurring in lower airways.

# Declarations

(i) This work has not previously been accepted in substance for any degree and is not being concurrently submitted in candidature for any degree.

Signed .....(candidate)

Date .....

(ii) This dissertation is the result of my own independent work/investigation, except where otherwise stated. Other sources are acknowledged by footnotes giving explicit references. A bibliography is appended.

Signed .....(candidate)

Date .....

(iii) I hereby give consent for my thesis, if accepted, to be available for photocopying and inter-library loan, and for the title and summary to be made available to outside organizations.

Signed .....(candidate)

Date .....

# Acknowledgements

I would like to express my sincere gratitude to my supervisors Prof. Perumal Nithiarasu and Dr. Raoul van Loon for their support and guidance throughout this work.

I would like to thank Dr. P. Ebdon, Dr. K. Lewis and Mr. M. Whittet for their advices on the human respiratory system.

The Erasmus Mundus funding provided by the European Commission that made my studies possible is gratefully acknowledged.

I thank all my teachers at CIMNE, Universitat Politecnica de Catalunya (UPC) and C2EC, Swansea University.

Sincere thanks to all my friends for their support and encouragements.

Words fail to express my utmost love to my family for their endless patience, love and encouragements.

To my family and the God I trust.

# Contents

Abstract.....	i
Declarations .....	ii
Acknowledgement.....	iii
Contents.....	iv
List of Figures .....	vi
List of Tables .....	vii
Symbols.....	viii
1. Introduction.....	1
1.1 Motivation.....	1
1.2 Anatomy of the lung .....	1
1.3 Physiology of the lungs .....	3
11.3.1 Mechanism of ventilation .....	4
1.3.1.1 Inhalation.....	4
1.3.1.2 Exhalation.....	4
1.3.1.3 Gas exchange .....	5
1.3.1.4 Blood circulation .....	6
1.3.2 Role of airways.....	7
1.3.1.1 Upper respiratory tract .....	7
1.3.1.2 Bronchial tree.....	7
1.3.1.3 Pulmonary acinus .....	8
1.3.3 Lung volumes .....	8
1.4 Disease states.....	10
1.5 Modelling .....	13
1.6 Outline of the thesis .....	2
2. Network Model.....	4
2.1 Governing 1D equations .....	2
2.2 The characteristic system.....	2

2.3 Boundary conditions .....	2
2.4 Discontinuities.....	2
2.5 Airway branching.....	2
2.6 Reflection .....	2
2.7 Finite element formulation.....	2
2.7.1 Temporal discretisation by Taylor-Galerkin scheme .....	3
2.7.2 Spatial discretisation .....	3
2.7.3 Stability and convergence .....	3
2.8 Programming.....	2
3. Model Problems .....	4
3.1 Introduction.....	2
3.2 Pulse propagation .....	2
3.3 Discontinuities.....	2
3.4 Branching.....	2
4. Results and Discussions .....	4
Type chapter title (level 2).....	5
Type chapter title (level 3).....	6
5. Conclusions and Future work .....	4
1.1 Conclusions .....	2
1.2 Future work .....	2
Bibliography .....	4

# List of Figures

1.1	A typical lung structure and its position in the respiratory system and structure of an alveolar sac .....	i
1.2	Weibel's model of branching airways .....	i
1.3	Typical respiratory cycle with a peak inlet flow rate of 1.4 l/s.....	i
1.4	Schematic diagram showing the flow of O <sub>2</sub> and CO <sub>2</sub> between the body tissues and the atmosphere...	i
1.5	Pulmonary circulation at Alveolar level .....	i
1.6	Typical spirometer trace showing the measurement of lung volumes .....	i
2.1	Nodal connection types of branching vessel segments .....	i
2.2	Mesh generation for the airway network model .....	i
2.3	Convergence of LCG method with increased spatial resolution.....	i
3.1 (a)	A Pulse propagation through a single vessel .....	i
3.1 (b)	Deformation (magnified 100 times) of the vessel with pressure intensities at time 0.02s, 0.04s, 0.05s during the first viscous flow case (case ii).....	i
3.2	Effect of sudden change in cross-sectional area in a single vessel.....	i
3.3	Effect of sudden change in material properties ( $\beta$ value) in a single vessel .....	i

# Symbols

$A$	Cross-sectional area	$\text{cm}^2$
$A_0$	Unstressed cross-sectional area	$\text{cm}^2$
$c$	Wave speed	$\text{cm/s}$
$c_0$	Intrinsic wave speed ( $c_0 = c$ when $A = A_0$ )	$\text{cm/s}$
$D$	Distensibility	
$E$	Elastic modulus	$\text{dyne/cm}^2$
$h$	Wall thickness	$\text{cm}$
$l_e$	Elemental length	$\text{cm}$
$L$	Segment length	$\text{cm}$
$n$	Current time step	
$p$	Mean internal pressure over a cross-section	$\text{dyne/cm}^2$
$p_{ext}$	External pressure	$\text{dyne/cm}^2$
$u$	Mean velocity of the flow over a cross-section	$\text{cm/s}$
$Q$	Volume flow rate	$\text{cm}^3/\text{s}$
$r$	Radial direction	$\text{cm}$
$t$	Time	$\text{s}$
$R$	Radius of the segment	$\text{cm}$
$R_r$	Reflection coefficient	(dimensionless)
$x$	Axial Direction	$\text{cm}$
$w$	Characteristic variable	$\text{cm/s}$
$w_{in}$	Incoming characteristic at the inlet	$\text{cm/s}$
$Y$	Characteristic admittance	
$Z$	Characteristic impedance	
<b>C</b>	Vector of source terms for the characteristic system	
$\mathbf{f}_\Gamma$	Vector of boundary flux terms for $\Omega$	
$\mathbf{f}_{\Gamma_e}$	Vector of boundary flux terms for $\Omega_e$	
<b>F</b>	Vector of conservation variables	
$\mathbf{F}_U$	$\mathbf{F}_U = \partial \mathbf{F} / \partial \mathbf{U} = \mathbf{H}$	
<b>H</b>	Jacobian matrix of the characteristic system	
<b>K, L</b>	Coefficient matrices for the LCG method	
$\mathbf{M}_e$	Mass matrix for the LCG method	
<b>N</b>	Finite element shape function	
<b>S</b>	Source term vector for the nonlinear system	
$\mathbf{S}_U$	$\mathbf{S}_U = \partial \mathbf{S} / \partial \mathbf{U}$	
<b>U</b>	Vector of primitive variables $\mathbf{U} = [A \ u]^T$	
$\alpha$	Womersley number	(dimensionless)
$\beta$	Material parameter of the vessel segments	
$\lambda_1, \lambda_2$	Eigenvalues of the characteristic system	
$\Gamma$	Boundary of the domain $\Omega$	
$\Gamma_e$	Boundary of the elemental sub-domain $\Omega_e$	
$\mu$	Fluid viscosity	poise
$\nu$	Kinematic viscosity	
$\rho$	Fluid density	$\text{g/cm}^3$
$\sigma$	Poisson ratio of the vessel wall	(dimensionless)
$\Omega, \Omega_e$	Global Domain & Elemental sub-domain	



# CHAPTER 1

## INTRODUCTION

### 1.1 MOTIVATION

The human respiratory system is one among the most intricate arts of nature. Like all the fields of sciences trying to understand the need based design of nature, a mathematician tries to understand the functional responses of the lungs to the various stimuli.

With the availability of high computing power, it has become possible to computationally model and study the airway geometry. The CFD simulations are widely used for predicting the gas transport, particle deposition and dosimetry of the human lung. Earlier simulations models were regular, dichotomous branching (Synder et al., 1981; Zhao and Lieber, 1994; Calay et al., 2002; Lee and Lee, 2002; Liu et al., 2003; Kleinstreuer and Zhang, 2003; Nowak et al., 2003; Shi et al., 2004; Zhang and Kleinstreuer, 2004). Recently, computational techniques are widely used to extract realistic 3D models of the lungs from the CT scan slices (Nowak et al. (2003) and Cebal and Summer (2004). But such models are limited because of the limitations on the resolution of the CT scans. Schmidt et al (2004) gave a digital reference model of the lungs. Calay has studied various respiratory flow patterns in realistic airway geometries. Liu et al. (2003) studied the 3D inspiratory flow in a 3D Weibel model. Some researchers have studied the particle deposition in the airways (Kleinstreuer and Zhang; 2003, van Ertbruggen et al. ;2005, Longest and Vinchurkar (2007b), Longest et al. (2006)). The Weibel model has been widely used despite it lacks information on the branching curvature and surface irregularities which are present in the airways. Cebal and Summer (2004) studied the airflow patterns in the central tracheal and bronchial airways down to 4 generations by using a virtual bronchoscopy reconstruction method. Longest and Vinchurkar (2007b) have studied the effects of upstream transition to turbulence on the flow field and particle deposition in the generations G3-G5 of the

respiratory tract. Kitaoka et al., 1999; Tawhai et al., 2000 and 2004; Spencer et al., 2001; Tgavalekos et al., 2003 ; Sera et al., 2003 ; Schmidt et al., 2004, have presented more realistic models using mathematical algorithms and new imaging techniques. Calay has used a 17 generation model to study the airflow.

## **1.2 ANATOMY OF THE LUNGS**

In human beings, the lungs are present in pairs and are located in the pleural cavities of the thorax on either side of the heart. Typical adult human lungs are about 25 to 30 cm long and are approximately cone shaped. The lungs are protected by a protective membrane called pulmonary pleura and are separated from the parietal pleura covering the chest wall by the pleural fluid. Both the lungs are separated by the mediastinum, which contains the heart, trachea, oesophagus and blood vessels. The lungs normally have clear anatomical divisions known as lobes (Ewart, 1889). The right lung is divided into three lobes viz., superior, middle and inferior lobes, by the oblique and horizontal fissures. While the left lung, which is slightly smaller, is divided into two lobes viz., superior and inferior lobes, by the oblique fissure. Figure 1.1 shows the location of the human lungs and its anatomical structure.

The trachea or the wind pipe leads the inhaled air from the larynx, into the conducting airways of the lungs which begin with the bifurcating bronchi. The first generation (or primary) of the bronchus leads the air into each of the lungs where they subdivide into secondary bronchi. The second generation (or secondary) bronchus leads into each of the lobes within which they subdivide into tertiary bronchus. These tertiary bronchi serve into each of the pyramid-shaped bronchopulmonary segments (Kramer, 1932) which are separated from one another by connective tissue septa. Each of these segment is served by its own artery and vein are clinically important because pulmonary disease is often confined to one or a few segments and these can be surgically removed without affecting the function of the other segments. Within these segments, the tertiary bronchi further subdivide in several generations of numerous smaller bronchioles. Weibel (1963) has observed 23 generations of conducting airways ranging from the trachea until the terminal bronchioles in normal human respiratory system. Figure 1.2 shows the Weibel observation of the airway branching.

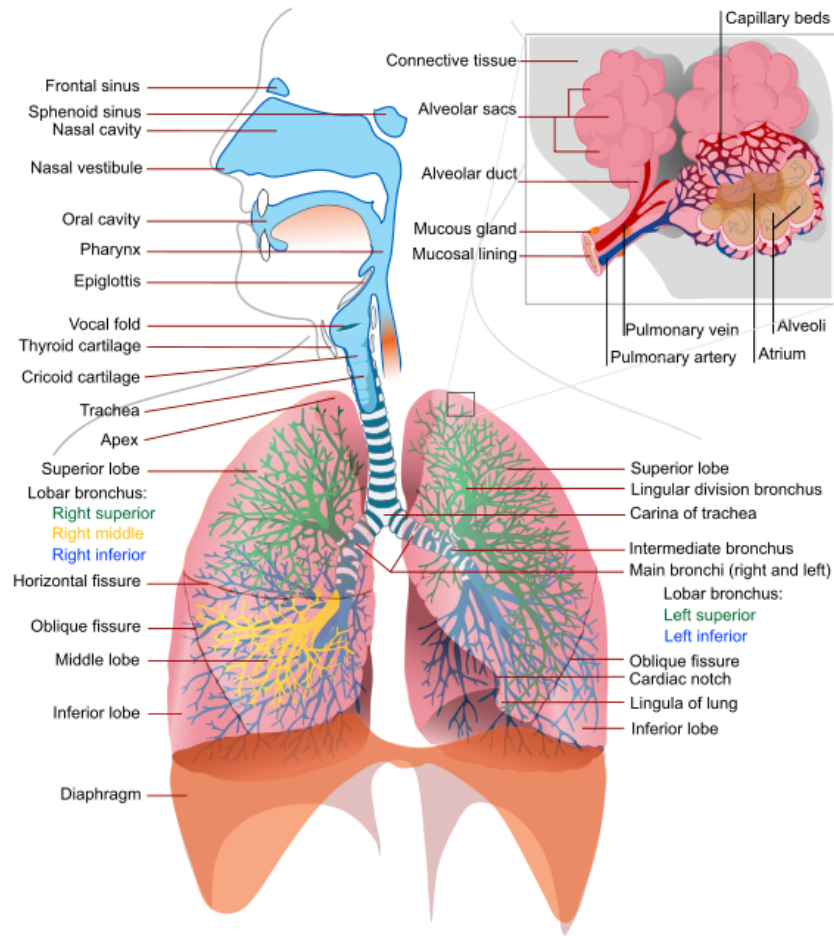


Figure 1.1 – A typical lung structure and its position in the respiratory system and structure of an alveolar sac  
(Source: Wikimedia)

These conducting airways lead into the respiratory zone of the lungs comprising of respiratory bronchioles, alveolar ducts and alveoli. The thin-walled sacs called alveoli are the respiratory surfaces of the lung. The alveolar ducts lead into a terminal bunch or into the alveolar sacs formed by a cluster of alveoli. It has been estimated that there are approximately 500 million alveolar sacs present in a human lung achieving an enormous surface area for gas exchange area of 50-100 square meters. Figure 1.4 shows a typical alveolar sac surrounded by the blood capillaries.


conducting zone	generation		diameter	length	number	total cross	Powder	
			(cm)	(cm)		sectional	deposition	
						area (cm <sup>2</sup> )	by particle	
conducting zone	trachea		0	1.80	12.0	1	2.54	7 - 10 μm
	bronchi		1	1.22	4.8	2	2.33	2 - 10 μm
			2	0.83	1.9	4	2.13	
			3	0.56	0.8	8	2.00	
	bronchioles		4	0.45	1.3	16	2.48	
			5	0.35	1.07	32	3.11	
terminal bronchioles	16	0.06	0.17	6 · 10 <sup>5</sup>	180.0			
transitional and respiratory zones	respiratory bronchioles	17	↓	↓	↓	↓	0.5 - 2 μm	
		18	↓	↓	↓	↓		
		19	0.05	0.10	5 · 10 <sup>5</sup>	10 <sup>3</sup>		
	alveolar ducts	20	↓	↓	↓	↓		
		21	↓	↓	↓	↓		
	22	↓	↓	↓	↓			
	alveolar sacs	23	0.04	0.05	8 · 10 <sup>6</sup>	10 <sup>4</sup>		

Figure 1.2 – Weibel's model of branching airways

### 1.3 PHYSIOLOGY OF THE LUNGS

The lungs are the major organs of the respiratory system and their main metabolic function is to facilitate the gas exchange between the lung and the atmosphere. The pulmonary ventilation in the lungs is the mechanical process by which the atmospheric air flows into and out of the lungs, which is achieved by the volumetric changes in the thoracic cavity. This volume change induces a negative alveolar pressure driving the air in during inhalation, and a positive alveolar pressure driving the air out during exhalation. The rate of ventilation is controlled by the autonomic nervous system from parts of the brain stem, the medulla oblongata and the pons. This comprises of two stages inspiration and expiration. Figure 1.3 shows a typical respiratory waveform with a peak flow rate of 1.4 l/s measured in Trachea.

## 1.3.1 MECHANISM OF VENTILATION

### 1.3.1.1 Inhalation

Under normal conditions, it is initiated by the contraction of the diaphragm and the contraction of the external intercostal muscles, elevating the ribs. The former allows the lung to expand downwards and the latter allows it to expand outwards. This causes a negative (suction) pressure difference of about 4mm Hg with respect to the atmospheric pressure (i.e.  $p_{pul} < p_{atm}$ ) to arise causing the air to flow in. The inspired air is filtered, warmed and humidified as it passes through the upper and lower conducting airways.

Normal resting respirations are 10 to 18 breaths per minute, with a time period of 2 seconds. During vigorous inhalation (at rates exceeding 35 breaths per minute), or in approaching respiratory failure, accessory muscles of respiration are recruited for support. These consist of sternocleidomastoid, platysma, and the scalene muscles of the neck. During forced inhalation, as when taking a deep breath, the external intercostal muscles and accessory muscles aid in further expanding the thoracic cavity.

### 1.3.1.2 Exhalation

Exhalation is generally a passive process achieved by the relaxation of the inspiratory muscles and the elastic recoil of the lungs. This decrease in the volume causes  $p_{pul} > p_{atm}$  by about 1mm Hg and the gases are forced out of the lungs until the pressures equilibrate. However, active or forced exhalation is achieved by the contraction of the abdominal and the internal intercostal muscles.

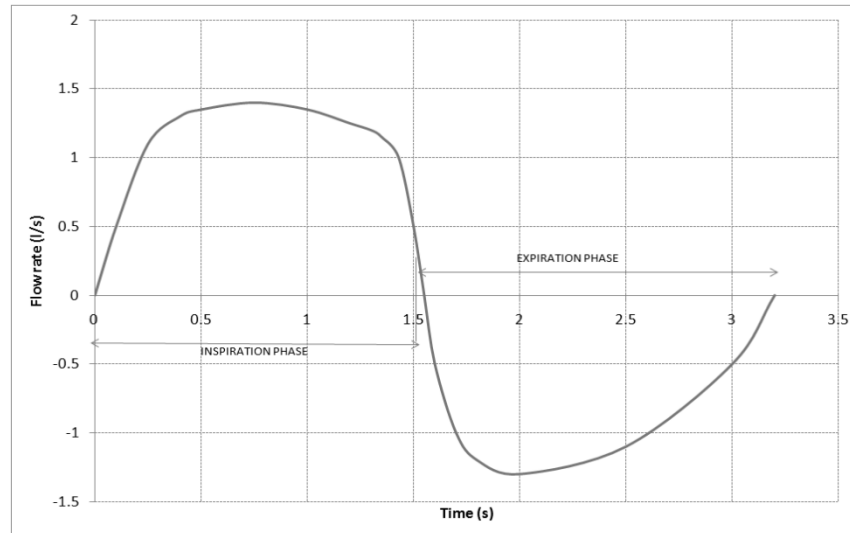


Figure 1.3 – Typical respiratory cycle with a peak inlet flow rate of 1.4 l/s

### 1.3.1.3 Gas exchange

Fick's law states that the rate of diffusion across a fluid membrane is directly proportional to the difference in the partial pressure of gases separated by the membrane, surface area of the membrane and inversely proportional to the wall thickness. As the air enters the respiratory zone, it fills up the alveolar sacs. The surfactant in the alveolar sac helps the tissues to reduce the surface tension and stretch further to achieve a significant increase in surface area (approximately  $100 \text{ m}^2$ ). The extremely thin (approx. 0.2 micrometres) alveolar walls are composed of a single layer of epithelial cells (type I and type II epithelial cells) in close proximity to the pulmonary capillaries which are composed of a single layer of endothelial cells. The velocity of the air entering the terminal bronchioles drop completely as it enters the alveoli and the gas exchange occurs due to passive diffusion. Thus, at normal resting conditions, the exchange of gases takes place by diffusion driven by the difference in the partial pressure of the gases. Thus, the  $\text{CO}_2$  with a high partial pressure ( $P_{\text{CO}_2} = 45 \text{ mm Hg}$ ) in the venous blood diffuses through the alveolar walls into the inspired air ( $P_{\text{CO}_2} = 40 \text{ mm Hg}$ ) and the lower partial pressure of  $\text{O}_2$  in the blood ( $P_{\text{O}_2} = 40 \text{ mm Hg}$ ) drives the  $\text{O}_2$  in air ( $P_{\text{O}_2} = 100 \text{ mm Hg}$ ) to dissolve into the blood. Similar diffusion of other metabolic wastes in the blood takes place. This gas exchange also serves to maintain the acid-base balance of the body.

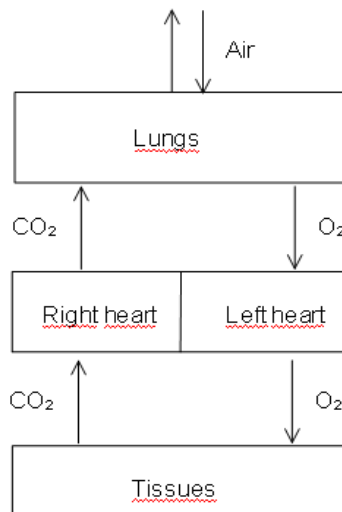


Figure 1.4 – Schematic diagram showing the flow of  $O_2$  and  $CO_2$  between the body tissues and the atmosphere

#### 1.3.1.4 Blood circulation

Pulmonary circulation dictates the blood flow between the heart and the lungs. The pulmonary artery serves the deoxygenated blood pumped from the heart to the lungs. The pulmonary artery divides in stages to first form the right and left pulmonary arteries and then into the lobar arteries and finally into the finer pulmonary capillaries which surround the alveolar surface. The oxygenated blood is then collected by the four pulmonary vein, which then serve the heart completing the circuit of pulmonary circulation. The numerous fine blood capillaries that are part of the pulmonary circulatory system absorb oxygen and eliminate  $CO_2$  depending on the metabolic demands of the cells in the body.

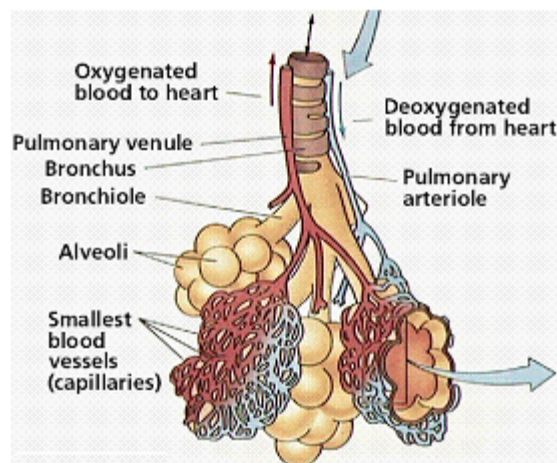


Figure 1.5 – Pulmonary circulation at Alveolar level (Source: Wikimedia)

## **1.3.2 ROLE OF THE AIRWAYS**

### **1.3.2.1 Upper respiratory tract**

In human beings, the air is inhaled through the nasal cavity and passes through the upper respiratory tract. The nasal cavity is equipped for warming, moistening and filtering the air before entering the lower airways. The walls of the cavity are lined by thin walled blood vessels for warming the air. The presence of fine hairs and lined with cells that secrete mucus and enzymatic serum each day serves the purpose of moistening the air as well as trapping any suspended particles. The gentle movement of the hair lining the vessels help to bring the suspended particles in the mucus to the throat which is removed by coughing out or swallowed to be removed through the digestive system.

The air then enters the Pharynx where any inhaled pathogens are destroyed by the lymphatic tissue. It then passes through to the laryngopharynx and larynx, which is responsible for controlling the airflow into the trachea and preventing food from entering it while swallowing. This is followed by the trachea which is also coated with cilia.

### **1.3.2.2 Bronchial tree**

The branching of the airways from the primary bronchi greatly influence further airflow. The successive branching of the airways result in the continuous increase in the total cross sectional area and the total conducting volume at each generation resulting in the mean velocity in Trachea which is about 100 cm/s drops down to 1 cm/s when it reaches the first order of terminal bronchioles [Weibel, 1994, Pedley 1970]. The resistance of the airflow depends on the diameter, location and the condition of the airways. In patients with respiratory disorders, the changes in the airway properties such as airway constriction, dilation or vessel softening or hardening will have an effect on the airflow through that broncho-pulmonary segment. In addition, the material properties of the airways vary depending on their generation, thus, the smaller airways tend to offer lower resistance compared to the ones higher up.



Moreover, the air occupied in the conducting airways (about 150 ml) do not take part in gas exchange and act like a reservoir. These parts of the respiratory tract starting from nose down to terminal bronchioles lacking respiratory acinus are called as anatomical deadspace.

### 1.3.2.1 Pulmonary acinus

As discussed earlier, alveoli form the respiratory acinus and this is where the gas exchange takes place. The thin alveolar walls and the extremely large surface area allow high rates of gas transfer to take place. At rest, a healthy human lung can give a total alveolar ventilation of about 8 litres of air per minute at the rate of 12 and 15 breaths per minute.

A healthy lung can conduct adequate gas transfer to maintain a cardiac output of over 20 litres per minute during exercise (Guyton, 1973) where as a diseased lung might conduct barely enough oxygenation at rest to support a cardiac output of only 5 litres per minute (Weitzenblum, 2002).

### 1.3.2 LUNG VOLUMES

Before discussing the mechanism of breathing, it is important to introduce the various capacities or volume measurements at various breathing states. These capacities can be measured by some of the known techniques such as Spirometry, Nitrogen washout, Helium dilution, Plethysmography, etc. Understanding of these capacities will assist in evaluating the health of the lung. As an effect of the lung diseases, some of these capacities will be reduced as a result.

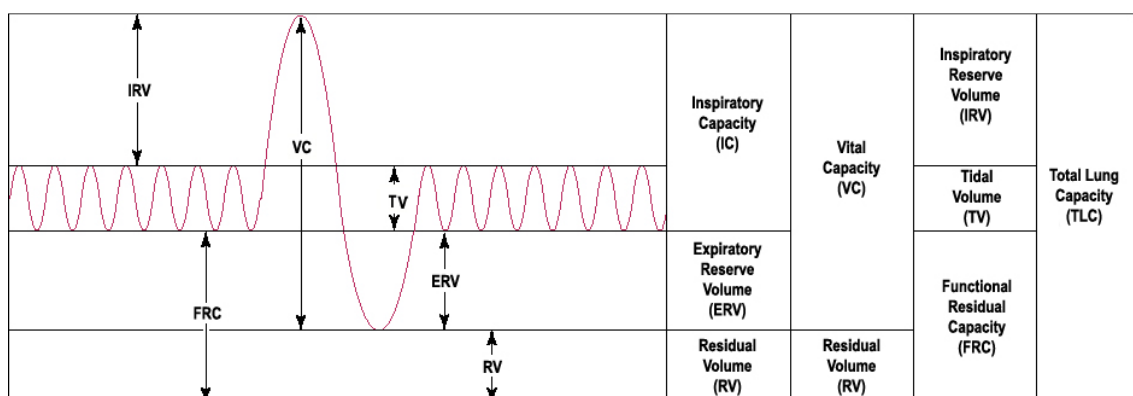


Figure 1.6 – Typical spirometer trace showing the measurement of lung volumes (Source: Wikipedia)

**Tidal volume (TV)** - It is the volume of air an individual breathes in or out during normal respiration. It is about 0.5 L in male and 0.39 L in female respectively. It can be measured using spirometry.

**Inspiratory reserve volume (IRV)** - It is the volume of air that can be breathed in during maximum inspiration in excess of the tidal volume. It is about 3 L in male and 2.3 L in female respectively. It can be measured using spirometry.

**Expiratory reserve volume (ERV)** - It is the volume of air that can be breathed out during maximum expiration in excess of the normal expiration limit. It is about 1.2 L in male and 0.93 L in female respectively. It can be measured using spirometry.

**Residual volume (RV)** - It is the volume of air left in the lungs after maximum expiration. It is about 1.2 L in male and 0.93 L in female respectively. It cannot be measured using spirometry.

**Inspiratory capacity (IC)** - The maximal volume of air that can be inspired following a normal expiration.  $IC = TV + IRV$

**Functional residual capacity (FRC)** - The volume of air that stays in the lungs during normal breathing.  $FRC = ERV + RV$ .

**Vital capacity (VC)** - The maximum volume of air that can be voluntarily moved in and out of the respiratory system.  $VC = IRV + TV + ERV$

**Total lung capacity (TLC)** - This is the total volume of the lung or the volume of air contained in the lung at the end of maximal inspiration.  $TLC = IRV + TV + ERV + RV$

## **1.4 RESPIRATORY DISEASES**

The respiratory system is exposed to the changes in the atmospheric air and also the various pollutants, harmful gases, suspended particles and various pathogens present in it. The respiratory diseases is a term denoting the diseases affecting the normal respiratory functions causing temporary or permanent impairment of the lung function. These diseases can affect whole or part of the lung that includes the upper respiratory tract, trachea, bronchi, pleural cavity, the control nerves and the muscles of breathing viz., diaphragm, intercostal muscles. These diseases range from mild and self-limiting such as the common cold to life-threatening such as bacterial pneumonia or pulmonary embolism. Some of the respiratory diseases are briefly discussed here [W1].

The respiratory diseases are broadly classified as obstructive diseases, restrictive diseases, respiratory tract infections, respiratory tumours, pleural cavity diseases, pulmonary vascular diseases, disorders of breathing mechanics.

### **1.4.1 Obstructive lung diseases**

They are characterized by the obstruction of the airways. Some examples are Asthma, bronchitis, COPD, Cystic fibrosis, etc.

#### **1.4.1.1 Chronic obstructive pulmonary disease (COPD)**

Chronic obstructive pulmonary disease (COPD), also known as chronic obstructive airways disease (COAD) or chronic airflow limitation (CAL) is a group of illnesses that includes chronic bronchitis and emphysema characterised by narrowing of airways limiting the airflow. It is caused by inhalation of toxic gases most commonly smoking. This causes inflammatory response in the airways known as chronic bronchitis or destruction of tissues leading to emphysema. It is one of the leading causes of death. The diagnosis can be done through lung performance test such as a peak flow meter or by spirometry.

#### **1.4.1.2 Asthma**

Asthma is an obstructive lung disease that has affected over 300 million people around the world. It is characterized by inflammation of airway leading to airway obstruction or extra sensitive (hyperresponsive) causing bronchospasm or wheezing. Asthma is usually triggered by certain allergens such as dust or pollen, upper respiratory tract infection, cold air, exercise or smoke leading to the inflammation and production of excess mucus and reducing the compliance of the airway. Asthma is a common condition and affects over 1 in 4 urban children [W1]. Asthmatics are known to experience wheezing, breathlessness, chest tightness, and coughing, particularly at night or in the early morning.

#### **1.4.1.3 Bronchitis**

Bronchitis is characterized by the inflammation of the major air passages within the lungs such as trachea and the large and small bronchi (airways) within the lungs become inflamed because of infection or other causes.

#### **1.4.1.4 Cystic fibrosis**

Cystic fibrosis is a genetic disorder of the cystic fibrosis transmembrane conductance regulator (CFTR) gene. This mutation of this gene causes reduced water content of secretions such as sweat mucus, etc. The thick viscous mucus secretion becomes hard to remove and makes the lungs more susceptible to infection, inflammation and mucous plugging.

#### **1.4.2 Restrictive lung diseases**

Restrictive lung diseases (also known as interstitial lung diseases) are characterized by a loss of lung compliance causing incomplete lung expansion and increased lung stiffness. E.g., infant respiratory distress syndrome (IRDS), Acute respiratory distress syndrome (ARDS), etc..

#### **1.4.3 Respiratory tract infections**

The respiratory tract infection are most commonly observed lung disease The most common upper respiratory tract infection is the common cold however infections of specific organs of the upper respiratory tract such as sinusitis, tonsillitis, otitis media,

pharyngitis and laryngitis are also considered upper respiratory tract infections. The most common lower respiratory tract infection is pneumonia, SARS, etc.

#### **1.4.6 Respiratory tumours**

Tumours [W1] of the respiratory system are either malignant or benign. Malignant tumors, or cancers of the respiratory system, are a major health problem responsible for 15% of all cancer diagnoses and 29% of all cancer deaths. The majority of respiratory system cancers are attributable to smoking tobacco. Benign tumors are relatively rare causes of respiratory disease. Examples of benign tumors are Pulmonary hamartoma, Congenital malformations such as pulmonary sequestration and congenital cystic adenomatoid malformation (CCAM).

#### **1.4.9 Pleural cavity diseases**

Pleural cavity diseases include empyema and mesothelioma. A collection of fluid in the pleural cavity is known as a pleural effusion. This may be due to fluid shifting from the bloodstream into the pleural cavity due to conditions such as congestive heart failure and cirrhosis or due to inflammation of the pleura itself as can occur with infection, pulmonary embolus, tuberculosis, mesothelioma and other conditions. A pneumothorax is a hole in the pleura covering the lung allowing air in the lung to escape into the pleural cavity causing the lung to deflate. When this air gets trapped, a tension pneumothorax develops causing pneumothorax to get bigger until it compresses the heart and blood vessels, leading to a life threatening situation.

#### **1.4.10 Pulmonary vascular diseases**

Pulmonary vascular diseases are conditions that affect the pulmonary circulation such as pulmonary embolism (when a blood clot embolizes in the pulmonary artery), pulmonary arterial hypertension (elevated pressure in the pulmonary arteries), pulmonary edema (leakage of fluid from capillaries of the lung into the alveoli) and pulmonary hemorrhage (inflammation and damage to capillaries in the lung resulting in blood leaking into the alveoli).

#### **1.4.11 Disorders of breathing mechanics**

Disorders of the brain's control of breathing, the nerves or the muscles of respiration can affect the respiratory system. Common disorders of breathing mechanics are obstructive sleep apnea, central sleep apnea, Amyotrophic lateral sclerosis, Guillan-Barre syndrome, and Myasthenia gravis.

Obesity is often associated with sleep apnea and can cause either an obstructive or a restrictive pattern on spirometry. Obesity reduces the movement of the chest wall which can, in extreme cases, result in the obesity-hypoventilation syndrome, a cause of respiratory failure.

# CHAPTER 2

# NETWORK MODEL

## 2.1 GOVERNING 1D EQUATIONS

In this model, the lower airways are idealised as one-dimensional tubular pathways with uniform initial cross sectional area and material characteristics at each of the segments. The flow through the airways is assumed laminar in this study, as discussed earlier [in chapter 1], which stands true for the flow past sixth generation as the  $Re \ll 2000$  [Ma 2006] and the turbulence effects in the fluid are observable in the earlier generations [ref]. In addition, the major interest of this study lies on the effect of the flow distribution due to the influence of branching networks and obstruction identification.

This idealisation of the airways, beginning from trachea, in 1D has been done ignoring the effects of the curvature of the vessels and assuming the fluid to be incompressible and Newtonian. The governing one-dimensional equations can be derived from the general mass and momentum conservation equations as shown below [Ref: Sherwin 2003, Mynard 2008]

$$\frac{\partial A}{\partial t} + \frac{\partial(Au)}{\partial x} = 0 \quad \dots \text{(Eq. 2.1)}$$

$$\frac{\partial u}{\partial t} + u \frac{\partial u}{\partial x} + \frac{1}{\rho} \frac{\partial p}{\partial x} - \frac{1}{\rho} \frac{\partial \tau}{\partial x} = 0 \quad \dots \text{(Eq. 2.2)}$$

where  $A$  is the cross-sectional area ( $\text{cm}^2$ ),  $u$  is the mean velocity over a cross section ( $\text{cm/s}$ ),  $p$  is the pressure ( $\text{dyne/cm}^2$ ),  $\rho$  is the density of the fluid ( $\text{g/cm}^3$ ) (approximately  $0.0012 \text{ g/cm}^3$  for air), and  $\tau$  is the shear stress component ( $\text{dyne/cm}^2$ ) which can be expressed as,  $\tau = \mu \left( \frac{\partial u}{\partial r} \right)_R$ , where  $\mu$  is the dynamic viscosity of the fluid (P or poise) (approximately  $1.824 \times 10^{-4} \text{ P}$  for air at  $20^\circ\text{C}$ ),  $r$  is the radial direction in three dimensional cylindrical coordinates, and  $R$  is the vessel radius.

Estimation of shear stress  $\tau$  also involves computing both its viscous and inertial components. The inertial components have been ignored in this study due to low Womersley parameter [J. R. Womersley. *An elastic tube theory of pulse transmission and oscillatory flow in mammalian arteries*. Technical Report TR 56-614, WADC Technical Report, 1957.]  $\alpha = R\sqrt{\omega\rho/\mu}$ , where  $\omega$  is the angular frequency of a given harmonic. For example, at Trachea with a diameter of 1.8 cm and assuming  $\omega = 5$  would result in  $\alpha = 5 < 10$ . And this value further goes down as the airway narrows. Hence, there is a possibility of the flow to fully develop with a parabolic wave front and the flow would be close to Poiseuille flow. Hence it is assumed that the flow will be fully-developed (i.e.  $\partial u/\partial x = 0$ ) and steady (i.e.  $\partial u/\partial t = 0$ ) flow which results in Poiseuille flow. The airflow through the airways depends on the driving pressure and the airway resistance,

$$Q = \frac{\Delta p}{R} = \frac{p_{atm} - p_a}{R} \quad \dots \text{(Eq. 2.3)}$$

where  $Q = Au$  is the rate of flow ( $\text{cm}^3/\text{s}$ ),  $p_{atm}$  is the atmospheric air pressure,  $p_a$  is the alveolar air pressure, airway resistance for circular tubes from Poiseuille's law will be,  $R = \frac{8\mu L}{\pi R^4}$  where,  $\mu = 1.827 \times 10^{-4}$  P is the dynamic viscosity of air at 20°C. Hence rewriting,

$$\frac{\Delta p}{L} = \frac{dp}{dx} = \frac{8\mu Q}{\pi R^4} = \frac{8\pi\mu u}{A} \quad \dots \text{(Eq. 2.4)}$$

Ignoring the inertial components of this flow, the frictional resistance is given by

$$f = \frac{\partial \tau}{\partial x} = \frac{8\pi\mu u}{A} \quad \dots \text{(Eq. 2.5)}$$

The above expressions will not be valid when the flow is non-Newtonian and becomes turbulent. In airways, though the turbulences do occur at larger airways it has been ignored in this study. The effect of turbulence shall be dealt in future work. In addition, the flow in the airways tends to become laminar at smaller airways.

Using Eq. 2.5 the momentum equation thus becomes as

$$\frac{\partial u}{\partial t} + u \frac{\partial u}{\partial x} + \frac{1}{\rho} \frac{\partial p}{\partial x} - \frac{8\pi\mu u}{\rho A} = 0 \quad \dots \text{(Eq. 2.3)}$$

To express this in terms of  $Q = Au$ , multiply both sides by  $A$



$$\frac{\partial Q}{\partial t} + \frac{\partial}{\partial x} \left( \alpha \frac{Q^2}{A} \right) + \frac{A}{\rho} \frac{\partial p}{\partial x} - K_R \frac{Q}{A} = 0 \quad \dots \text{(Eq. 2.4)}$$

where,  $K_R = \frac{8\pi\mu}{\rho}$

Here  $\alpha$  is the Coriolis coefficient [(Canic and Kim 2003)]. Replacing  $Q = Au$

$$\frac{\partial(Au)}{\partial t} + \frac{\partial}{\partial x} (\alpha Au^2) + \frac{A}{\rho} \frac{\partial p}{\partial x} + K_R u = 0 \quad \dots \text{(Eq. 2.5)}$$

expanding with the product rule and factorizing

$$u \left( \frac{\partial A}{\partial t} + \frac{\partial}{\partial x} (\alpha Au) \right) + A \frac{\partial u}{\partial t} + \alpha Au \frac{\partial u}{\partial x} + \frac{A}{\rho} \frac{\partial p}{\partial x} + K_R u = 0 \quad \dots \text{(Eq. 2.6)}$$

when  $\alpha = 1$ , using Eq. 2.1, the above equation reduces to,

$$A \frac{\partial u}{\partial t} + Au \frac{\partial u}{\partial x} + \frac{A}{\rho} \frac{\partial p}{\partial x} + K_R u = 0 \quad \dots \text{(Eq. 2.7)}$$

divide by  $A$  gives

$$\frac{\partial u}{\partial t} + u \frac{\partial u}{\partial x} + \frac{1}{\rho} \frac{\partial p}{\partial x} + K_R \frac{u}{A} = 0 \quad \dots \text{(Eq. 2.8)}$$

or equivalently

$$\frac{\partial u}{\partial t} + \frac{1}{2} \frac{\partial u^2}{\partial x} + \frac{1}{\rho} \frac{\partial p}{\partial x} + K_R \frac{u}{A} = 0 \quad \dots \text{(Eq. 2.9)}$$

The pressure term can be expressed in terms of area  $A(x)$ , wall properties  $\beta(x)$  and equilibrium area  $A_0(x)$  using

$$\frac{\partial p}{\partial x} = \frac{\partial p}{\partial A} \frac{\partial A}{\partial x} + \frac{\partial p}{\partial \beta} \frac{\partial \beta}{\partial x} + \frac{\partial p}{\partial A_0} \frac{\partial A_0}{\partial x} \quad \dots \text{(Eq. 2.11)}$$

Where the wall property  $\beta$  given by [Formaggia] has been used

$$\beta = \frac{\sqrt{\pi} h_0 E}{(1-\nu)^2 A_0} \quad \dots \text{(Eq. 2.12)}$$

where  $h_0$  is the wall thickness in cm,  $E$  is the Elastic modulus,  $\nu$  is the poisson's ratio,  $A_0$  is the intial cross sectional area in  $\text{cm}^2$ .

The constitutive equation defining the relation between pressure and area given by [Sherwin] has been used in this study

$$p = p_{ext} + \beta \left( \sqrt{A} - \sqrt{A_0} \right) \quad \dots \text{(Eq. 2.13)}$$

From the above equation, it can be derived that,

$$\frac{\partial p}{\partial A} = \frac{\beta}{2\sqrt{A}} \quad \dots \text{(Eq. 2.14)}$$

Eq. 2.13 can also be rewritten to express Area in terms of pressure,

$$A = \left( \frac{p - p_{ext}}{\beta} + \sqrt{A_0} \right)^2 \quad \dots \text{(Eq. 2.15)}$$

Substituting Eq. 2.11 into Eq. 2.2 and also using Eq. 2.14 gives

$$\frac{\partial u}{\partial t} + \frac{1}{2} \frac{\partial u^2}{\partial x} + \frac{1}{\rho} \left( \frac{\beta}{2\sqrt{A}} \frac{\partial A}{\partial x} + \frac{\partial p}{\partial \beta} \frac{\partial \beta}{\partial x} + \frac{\partial p}{\partial A_0} \frac{\partial A_0}{\partial x} \right) = 0 \quad \dots \text{(Eq. 2.16)}$$

If  $\beta$  and  $A_0$  are constant along the vessel, and given that

$$c^2 = \frac{A}{\rho} \frac{\partial p}{\partial A},$$

$$c = \sqrt{\frac{\beta \sqrt{A}}{2\rho}} \quad \dots \text{(Eq. 2.17)}$$

where  $c$  is the intrinsic wave speed. It should be noted that [Mynard ] the finite amplitude pulses travel at a speed of  $|u+c|$  rather than  $c$ . Since the airways comprise of shorter vessels and the frequency of breathing is sufficiently large such that the possibility of shock formation is very little.

We can then reduce Eq. 2.16 using Eq. 2.17 into,

$$\frac{\partial u}{\partial t} + \frac{1}{2} \frac{\partial u^2}{\partial x} + \frac{c^2}{A} \frac{\partial A}{\partial x} = 0 \quad \dots \text{(Eq. 2.18)}$$

The above Eq. 2.18 combined with continuity equation (Eq. 2.1), the system of nonlinear equations can be written in quasi-linear form,

$$\frac{\partial \mathbf{U}}{\partial t} + \mathbf{H} \frac{\partial \mathbf{U}}{\partial x} = \mathbf{f} \quad \dots \text{(Eq. 2.19)}$$

where  $\mathbf{U} = \begin{bmatrix} A \\ u \end{bmatrix}$  and  $\mathbf{H} = \begin{bmatrix} u & A \\ c^2/A & u \end{bmatrix}$

If we assume  $\beta$  and  $A_0$  are constant and  $K_R = 0$ ,  $\mathbf{f} = 0$ , otherwise

$$\mathbf{f} = \begin{bmatrix} 0 \\ K_R \frac{u}{A} - \frac{\partial p}{\partial \beta} \frac{\partial \beta}{\partial x} + \frac{\partial p}{\partial A_0} \frac{\partial A_0}{\partial x} \end{bmatrix}$$

In conservation form, this is

$$\frac{\partial \mathbf{U}}{\partial t} + \frac{\partial \mathbf{F}}{\partial x} = \mathbf{S} \quad \dots \text{(Eq. 2.20)}$$

where  $\mathbf{U} = \begin{bmatrix} A \\ u \end{bmatrix}$  and  $\mathbf{F} = \begin{bmatrix} uA \\ \frac{u^2}{2} + \frac{p}{\rho} \end{bmatrix}$  and  $\mathbf{S} = \begin{bmatrix} 0 \\ -K_R \frac{u}{A} \end{bmatrix}$

## 2.2 THE CHARACTERISTIC SYSTEM

[Formaggia \*et al.\*\[\],](#) [Sherwin \*et al.\*\[\],](#) [Mynard \*et al.\*\[\]](#) have analysed the characteristics of the flow governed by the set of nonlinear equations given in Eq. 2.20. It can be shown from the quasi linear form of the system of equations given in Eq. 2.19 that the characteristic system can be derived as,

$$\frac{\partial w_i}{\partial t} + \lambda_i \frac{\partial w_i}{\partial x} = 0 \quad \dots \text{(Eq. 2.21)}$$

and the characteristic variables can be shown as

$$\begin{bmatrix} w_1 \\ w_2 \end{bmatrix} = \begin{bmatrix} u + 4c \\ u - 4c \end{bmatrix} \quad \dots \text{(Eq. 2.22)}$$

where  $w_1$  and  $w_2$  represent the forward and backward travelling wave fronts respectively.

Also, the eigenvalues of the Eq. 2.19 can be shown as,

$$\Lambda = \begin{bmatrix} \lambda_1 \\ \lambda_2 \end{bmatrix} = u \pm \sqrt{\frac{\beta \sqrt{A}}{2\rho}} = \begin{bmatrix} u + c \\ u - c \end{bmatrix} \quad \dots (\text{Eq. 2.23})$$

Thus, the primitive variables can be calculated from the characteristic equations as,

$$A = \frac{(w_1 - w_2)^4}{1024} \left( \frac{\rho}{\beta} \right)^2 \quad \dots (\text{Eq. 2.23})$$

$$u = (w_1 + w_2)/2 \quad \dots (\text{Eq. 2.24})$$

The characteristic system gives the forward and backward component of the propagation speed of the wave fronts [Mynard]. It should be noted that the wave fronts refers to the infinitesimal change in the characteristic variables  $w_1$  or  $w_2$ . In the network model, whenever there is a change in the vessel properties or branching it will affect the characteristic impedance and cause the wavefronts to reflect.

## 2.3 BOUNDARY CONDITIONS

The flow through the respiratory system is subsonic ( $u < c$ ), therefore, one boundary condition needs to be specified at both the inlet and the outlet. It is possible to prescribe both reflecting and non-reflecting boundary conditions. In this study, non reflecting boundary conditions [Mynard 2008] which can be easily computed using the characteristic system has been used and shall be discussed in this section. This involves calculating the forward ( $w_1$ ) and backward travelling wavefronts ( $w_2$ ). For the time step 'n+1', the outgoing characteristic at the inlet and exit may be calculated via linear extrapolation in the x-t plane,

$$w_2^{n+1} \Big|_{x=x_0} = w_2^n \Big|_{x=x_0} - \lambda_2^n \Delta t \quad \dots (\text{Eq. 2.25})$$

$$w_1^{n+1} \Big|_{x=x_L} = w_1^n \Big|_{x=x_L} - \lambda_1^n \Delta t \quad \dots (\text{Eq. 2.26})$$

at the inlet and outlet respectively, where  $x_0$  and  $x_L$  are the coordinates of the inlet and outlet.

As said earlier, the non reflecting boundary conditions involve prescribing at the inlet the forward component of the pressure, area or velocity. This is achieved by prescribing the incoming characteristic ( $w_1$ ) [Formaggia et al.]. Thus to prescribe forward component of area at  $(n+1)^{\text{th}}$  time step, rearranging Eq. 2.23 yields,

$$w_{1,in}^{n+1} = w_2^0 + 8 \left( \bar{A}^{n+1} \right)^{1/4} \sqrt{\frac{\beta}{2\rho}} \quad \dots \text{(Eq. 2.27)}$$

To prescribe forward component of pressure at  $(n+1)^{\text{th}}$  time step, substituting the P-A relationship (Eq. 2.15) into (Eq. 2.24)

$$w_{1,in}^{n+1} = w_2^0 + 4 \sqrt{\frac{2}{\rho}} \sqrt{(\bar{p}^{n+1} - p_{ext}) + \beta \sqrt{A_0}} \quad \dots \text{(Eq. 2.28)}$$

Finally, forward component of velocity at  $(n+1)^{\text{th}}$  time step may be prescribed by rearranging (Eq. 2.24)

$$w_{1,in}^{n+1} = 2\bar{u}^{n+1} - w_2^0 \quad \dots \text{(Eq. 2.29)}$$

It should be noted that  $w_2^0$  is the initial value of  $w_2$  and will be equal to  $w_2$  until a backward running wave reach inlet. The backward running component of the variables can be prescribed in a similar fashion.

## 2.4 DISCONTINUITIES

The term discontinuity refers to the sudden changes in the cross-sectional properties such as area ( $A_0$ ), material parameters ( $\beta$ ) which depend on the wall thickness, Elastic modulus of the vessel segment and Poisson's ratio or branching of vessels. [Section 2.6](#) deals with the influence of material and geometric discontinuities on the characteristic impedance of the system, which will cause formation of partial or full reflection of the transmitted wave. In [section 2.5](#), discontinuities arising out of branching of airway segments is discussed.

## 2.5 AIRWAY BRANCHING

Beginning from Trachea, the airways start to branch out into two or several daughter branches. There is no particular order to this branching if the branches beyond the first few generations are considered [[Horsfield](#)]. In this study, mainly a maximum three daughter airways are considered to branch for a parent airway. As discussed in the previous section, these branching points can cause geometric or material discontinuity. However, this is not difficult to address in LCG method, which permits several nodes of the daughter segments to share the same location, which is especially useful at the branching locations. [Figure 2.1](#)

illustrates some of the possible 1D airway branching addressed in this code. However, it should be noted that the effects of branching angles has been reserved for future studies.

At these branching locations, it is worthwhile to mention that it is possible to have any number of branching segments complying with the mass and momentum continuity conditions. Thus, a system of nonlinear equations [Mynard, 2008] can be written based on the outgoing characteristics, conservation of mass and momentum equations as below, which are solved using Newton-Raphson method.

The characteristic for the nodes in the parent airway can be written as ,

$$w_{1p} = u_p + 4A_p^{1/4} \sqrt{\frac{\beta_p}{2\rho}} \quad \dots \text{(Eq. 2.30)}$$

and for the nodes in the  $d^{\text{th}}$  daughter vessel can be written as,

$$w_{2d} = u_d + 4A_d^{1/4} \sqrt{\frac{\beta_d}{2\rho}} \quad \dots \text{(Eq. 2.31)}$$

Mass conservation and pressure continuity equations can then be written as,

$$Q = A_p u_p = \sum_{d=1}^N A_d u_d \quad \dots \text{(Eq. 2.32)}$$

$$\frac{\rho u_p^2}{2} + p_{ext,p} + \beta(\sqrt{A_p} - \sqrt{A_{p0}}) = \frac{\rho u_d^2}{2} + p_{ext,d} + \beta(\sqrt{A_d} - \sqrt{A_{d0}}) \quad \dots \text{(Eq. 2.34)}$$

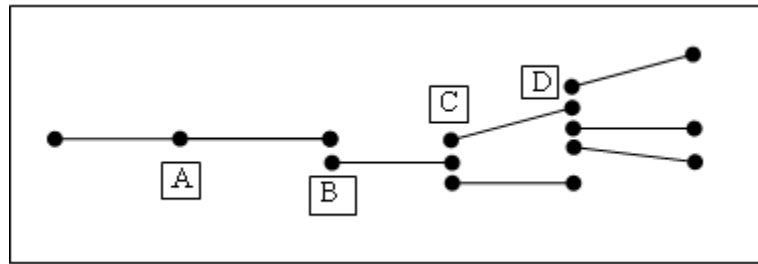


Figure 2.1 – Nodal connection types of branching vessel segments

## 2.6 REFLECTION

Whenever there is a change in the characteristic impedance due to the changes in cross-sectional area, vessel properties or vessel branching, there is bound to be a reflection of the

transmitted wave at these locations. In this code [Mynard], it is addressed with the help of the well-known linear transmission theory.

The characteristic impedance relates the wave velocity with the applied pressure and can be written as,

$$Z_0 = \frac{1}{Y_0} = \frac{\rho c_0}{A_0} = \frac{\sqrt{\rho\beta}}{\sqrt{2}A_0^{3/4}} \quad \dots \text{(Eq. 2.35)}$$

where  $Z_0$  is the characteristic impedance,  $Y_0$  is the characteristic admittance,  $c_0$  is the wave speed.

The ratio of the amplitudes of the transmitted and the reflected wave is commonly referred to as the reflection coefficient ( $R_t$ ) [Mynard]. It can be expressed in terms of characteristic admittance in linear form [Mynard] as,

$$R_t = \frac{Y_{op} - \sum Y_{od}}{Y_{op} + \sum Y_{od}}, \quad 0 \leq R \leq 1 \text{ for any } Y_{op} \geq 0 \quad \dots \text{(Eq. 2.36)}$$

where the  $Y_{op}$  and  $Y_{od}$  are the characteristic admittance of the parent and daughter vessels respectively. It is interesting to note that this can also be used to define the boundary conditions of the terminal vessels.

## 2.7 FINITE ELEMENT FORMULATION

The finite element formulation of the problem has been shown in involves the spatial and temporal discretisation of the partial differential equations over the domain under consideration. It has been shown in several instances including the network model of blood flow [Mynard 2008] that the standard Galerkin method cannot be used due to the convective term, which will cause spatial instability. A suitable alternative would be the Taylor Galerkin method that gives a better spatial stability. In this study, specifically, the choice of locally conservative Taylor Galerkin method is quite apparent to avoid the computation involving inversion of large matrices that would otherwise be needed. Also, the method has been shown to be stable and robust in solving the Blood flow problem by Mynard [2008]. Following the work of Mynard *et al.* the formulation of Locally conservative Taylor Galerkin method is shown here.

### 2.7.1 TEMPORAL DISCRETISATION BY TAYLOR GALERKIN SCHEME

The Taylor Galerkin temporal discretization of the U-A system have already been derived by [Formaggia et al.](#) and [Sherwin et al.](#) The U-A system in conservation form from Equation 2.20 is

$$\frac{\partial \mathbf{U}}{\partial t} + \frac{\partial \mathbf{F}}{\partial x} = \mathbf{S} \quad \dots \text{(Eq. 2.37)}$$

where  $\mathbf{U}$ ,  $\mathbf{F}$  and  $\mathbf{S}$  are the vectors of primitive variables, conservative variables and the source term respectively.

Rearranging gives, 
$$\frac{\partial \mathbf{U}}{\partial t} = \mathbf{S} - \frac{\partial \mathbf{F}}{\partial x} \quad \dots \text{(Eq. 2.38)}$$

Differentiating with respect to time,  $t$  and applying the chain rule yields the following equation,

$$\frac{\partial^2 \mathbf{U}}{\partial t^2} = \mathbf{S}_u \frac{\partial \mathbf{U}}{\partial t} - \frac{\partial}{\partial x} \left( \mathbf{F}_u \frac{\partial \mathbf{U}}{\partial t} \right) \quad \dots \text{(Eq. 2.39)}$$

where  $\mathbf{F}_u = \frac{\partial \mathbf{F}}{\partial \mathbf{U}}$  and  $\mathbf{S}_u = \frac{\partial \mathbf{S}}{\partial \mathbf{U}}$ . Substituting Eq. 2.38 in Eq. 2.39 will help to eliminate the time derivatives and gives,

$$\frac{\partial^2 \mathbf{U}}{\partial t^2} = \mathbf{S}_u \left( \mathbf{S} - \frac{\partial \mathbf{F}}{\partial x} \right) - \frac{\partial (\mathbf{F}_u \mathbf{S})}{\partial x} + \frac{\partial}{\partial x} \left( \mathbf{F}_u \frac{\partial \mathbf{F}}{\partial x} \right) \quad \dots \text{(Eq. 2.40)}$$

For time discretisation, consider the Taylor series expansion

$$\mathbf{U}^{n+1} = \mathbf{U}^n + \Delta t \frac{\partial \mathbf{U}^n}{\partial t} + \frac{\Delta t^2}{2} \frac{\partial^2 \mathbf{U}^n}{\partial t^2} + O(\Delta t^3) \quad \dots \text{(Eq. 2.41)}$$

where  $\Delta t$  is the time step and  $n$  refers to the current time step. By substituting the time derivatives obtained earlier in Eqs. 2.39 & 2.40 and ignoring higher order terms gives

$$\mathbf{U}^{n+1} = \mathbf{U}^n + \Delta t \left( \mathbf{S}^n - \frac{\partial \mathbf{F}^n}{\partial x} \right) + \frac{\Delta t}{2} \left[ \frac{\partial}{\partial x} \left( \mathbf{F}_u^n \mathbf{S}^n - \mathbf{F}_u^n \frac{\partial \mathbf{F}^n}{\partial x} \right) + \mathbf{S}_u^n \frac{\partial \mathbf{F}^n}{\partial x} - \mathbf{S}_u^n \mathbf{S}^n \right] \dots \text{(Eq. 2.42)}$$

The second bracketed term is the Taylor- Galerkin stabilization term.



## 2.7.2 SPATIAL DISCRETISATION

The Locally conservative galerkin method or LCG introduced by Nithiarasu [N1] and Thomas[T1, T2, T3] and is preferred for the spatial discretization of the domain  $\Omega$  with boundaries  $\Gamma$ . This method is much preferred for network models [Mynard] as it eliminates large matrix operations which is inevitable in global Galerkin method. Apart from that, it can handle discontinuities very well as in this method each element is treated as a sub-domain within its boundaries. The LCG discretisation for a inviscid case shown by Mynard *et al.* is shown here for completeness.

Using the standard finite element formulation for linear spatial discretisation, the weak form of Eq. 2.31 using a linear approximation function  $\hat{\phi} = N_i \tilde{\phi}_i + N_j \tilde{\phi}_j$ , where  $N_i = (x_j - x) / (x_j - x_i)$  and  $N_j = (x - x_i) / (x_j - x_i)$  and a Galerkin weighting  $\mathbf{N}^T$  gives,

$$\int_{\Omega_e} \left( \mathbf{N}^T \frac{\Delta \hat{\mathbf{U}}^n}{\Delta t} - \mathbf{N}^T \hat{\mathbf{R}}_h^n \right) d\Omega = 0 \quad \dots \text{(Eq. 2.43)}$$

where  $\mathbf{R}_h$  denote the right hand terms.

Eq. 2.31 can be written in a compact form as

$$[\mathbf{M}_e] \{\Delta \mathbf{U}\} = \Delta t ([\mathbf{K}_c] \{\mathbf{F}\}^n + [\mathbf{L}_e] \{\mathbf{S}\}^n + \{\mathbf{f}_{\Gamma_c}\}^n) \quad \dots \text{(Eq. 2.44)}$$

where  $[\mathbf{M}]$  is the mass matrix and  $[\mathbf{K}]$  and  $[\mathbf{L}]$  are the coefficient matrices for convection, Taylor-Galerkin and source terms. They are  $N_{\text{nodes}} \times N_{\text{nodes}}$  matrices, where  $N_{\text{nodes}}$  is the number of nodes in the domain  $\Omega$ . Also,  $\Delta \mathbf{U} = \mathbf{U}^{n+1} - \mathbf{U}^n$  and  $\mathbf{f}$  contains the boundary fluxes.

The reduced form of Eq. 2.43 after removing the viscous terms involving  $\mathbf{S}$  and  $\mathbf{S}_U$  gives,

$$\int_{\Omega_e} \mathbf{N}^T \frac{\Delta \hat{\mathbf{U}}^n}{\Delta t} = - \int_{\Omega_e} \mathbf{N}^T \frac{\partial \hat{\mathbf{F}}^n}{\partial x} d\Omega_e + \frac{\Delta t}{2} \int_{\Omega_e} \mathbf{N}^T \frac{\partial}{\partial x} \left( \hat{\mathbf{F}}^n \mathbf{U} \frac{\partial \hat{\mathbf{F}}^n}{\partial x} \right) d\Omega_e = 0 \quad \dots \text{(Eq. 2.45)}$$

Integrating the terms, results in the following elemental matrices. The consistent element mass matrix will be,

$$[\mathbf{M}_e] = \frac{l_e}{6} \begin{bmatrix} 2 & 1 \\ 1 & 2 \end{bmatrix} \quad \dots \text{(Eq. 2.46)}$$

where,  $l_e$  is the element length. The coefficient matrix  $[\mathbf{K}_e]$  is found to be

$$[\mathbf{K}_e] = \left( \frac{1}{2} + \frac{\Delta t}{4} \tilde{\mathbf{S}}^n_{\mathbf{u}} \right) \begin{bmatrix} -1 & -1 \\ 1 & 1 \end{bmatrix} - \frac{\Delta t}{2l_e} \tilde{\mathbf{F}}^n_{\mathbf{u}} \begin{bmatrix} 1 & -1 \\ -1 & 1 \end{bmatrix} \quad \dots \text{(Eq. 2.47)}$$

Where,  $\tilde{\mathbf{F}}_{\mathbf{u}}$  and  $\tilde{\mathbf{S}}_{\mathbf{u}}$  are average values over the elemental sub-domain.

The coefficient matrix  $[\mathbf{L}_e]$  is found to be

$$[\mathbf{L}_e] = \left( \frac{l_e}{6} + \frac{\Delta t l_e}{12} \tilde{\mathbf{S}}^n_{\mathbf{u}} \right) \begin{bmatrix} 2 & 1 \\ 1 & 2 \end{bmatrix} + \frac{\Delta t}{4} \tilde{\mathbf{F}}^n_{\mathbf{u}} \begin{bmatrix} -1 & -1 \\ 1 & 1 \end{bmatrix} \quad \dots \text{(Eq. 2.48)}$$

Finally, writing the flux term without including the contributions of the TG terms since they arise from the numerical technique and will be zero on the boundaries,

$$\{\mathbf{f}_e\} = \begin{Bmatrix} \tilde{\mathbf{F}}_i^n \\ -\tilde{\mathbf{F}}_j^n \end{Bmatrix} \quad \dots \text{(Eq. 2.49)}$$

The values from Eqs. 2.46 – 2.49 can be substituted in Eq. 2.44 to complete the formulation. Figure 2.2 shows a typical 1D mesh generated for a three generation network model. It can be seen that multiple nodes can be placed at the same branching points.

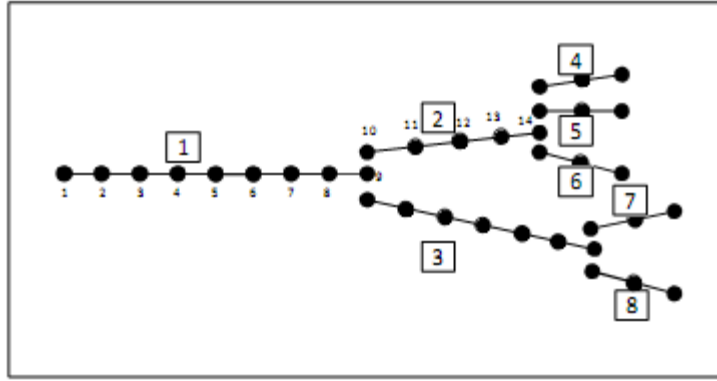


Figure 2.2 – Mesh generation for the airway network model

### 2.7.3 STABILITY AND CONVERGENCE

It has been shown that [Thomas, Mynard] that by assuming  $u \ll c$ , the stability condition for the characteristic system is

$$\Delta t_{\max} \approx \frac{\Delta x_{\min}}{c_{\max}} \quad \dots \text{(Eq. 2.50)}$$

Figure 2.3 shows the spatial convergence of the method as the element sizes are reduced from  $L/6$  to  $L/100$  where  $L$  is the domain length. The error is computed with respect to the amplitude of the peak pressure measured for the smallest element size of  $L/100$  and smallest time step of  $1\mu\text{s}$ . It may be noted that the error is negligibly small below a mesh size of  $L/20$ .

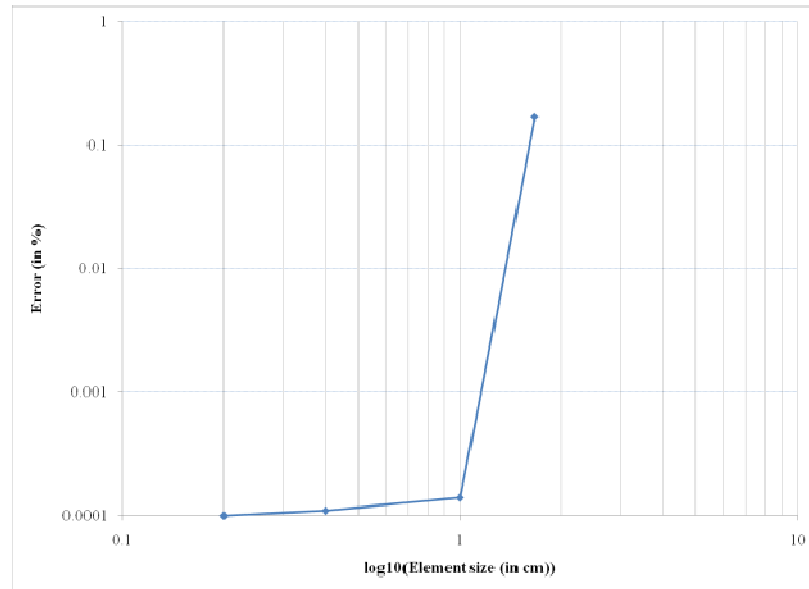


Figure 2.3 – Convergence of LCG method with increased spatial resolution.  
 [Note: Error is calculated based on the peak pressure value for the smallest mesh size with the smallest time step of  $1\mu\text{s}$ ]

## 2.8 PROGRAMMING

The code developed for the 1D network model of blood flow [Mynard 2008] was modified to study the respiratory flow through the 1D network model of the human lower airways. The code is based on the Locally conservative Taylor Galerkin method [Mynard, Thomas] which has been discussed in section 2.7. The basic framework of the pre-processor, solver and a postprocessor is discussed in this section.

### 2.8.1 PRE-PROCESSING STAGE

1. Creation of the input files.
  - a. Creation of the input files i. for the definition of the geometric and material properties of the numerous branching segments and definition of their daughter segments, ii. for the definition of the input respiratory waveform

based on the values of pressure at various instance of the respiratory phase measured at the inlet of the trachea.

2. Mesh generation.
  - a. 1D mesh is then generated based on the geometric, material and connectivity details in the input files and is written in a separate file to be used by the main program.
3. Computation
  - a. Based on the 1D mesh generated, the elemental mass matrices and their inverses are computed
  - b. Based on the input waveform, the initial incoming characteristics at the inlet for each time step is calculated

### **2.8.2 MAIN PROCESSING STAGE**

At every time step, the following computations are performed

1. The outgoing characteristics at the inlet are calculated
2. The boundary conditions are assigned based on the incoming and outgoing characteristics
3. The boundary conditions for all the co-located nodes at each of the discontinuity or branching point are calculated
4. The governing equations are solved using the LCG method

### **2.8.3 POST-PROCESSING**

1. At the assigned monitoring points, the values of the pressure, velocity, area and flow rate that are stored in an output file for post-processing.
2. These data from the output file are then read to generate the computed waveforms at the monitored points for further observation or studies.
3. This output data is be used to create 3D representation of the computed variables.

# CHAPTER 3

## MODEL PROBLEMS

### 3.1 INTRODUCTION

In this chapter, some model problems are shown to demonstrate the capability of the 1D LCG code for the network model. The models are chosen from the 1D test models used by [Mynard 2008, Sherwin 2003, Formaggia 2002]. In section 3.2, the propagation of a pressure wave in an isolated Gaussian pulse form and an inspiratory wave form are shown. A 3D representation of the result is also shown to complement the plots for better understanding. In section 3.3, the model problems are chosen to demonstrate the reflecting waves due to discontinuities in the model. In section 3.4, a simple branching model is used to explain the possible outcomes of a fluid flow through a branching model.

### 3.2 PULSE PROPAGATION

In this section, the propagation of a pressure pulse through a vessel segment of length,  $l = 12$  cm and initial cross-sectional area,  $A_0 = 1.0$  cm<sup>2</sup> and  $\beta = 226974$  dyne/cm<sup>2</sup> is demonstrated. Figure 3.1 shows the propagation of a pressure pulse with Gaussian distribution across a frequency of 0.03 s and a peak value of 1000 dyne/cm<sup>2</sup>. The cases studied are Ñ i. No viscosity (inviscid), ii. Viscous flow with a viscosity of 0.035 P and density 1.06 g/cm<sup>3</sup>, and iii. Viscous flow with a viscosity of  $1.84 \times 10^{-4}$  P and density 0.0012 g/cm<sup>3</sup>.

The following observations can be made from the Figure 3.1a which shows the pressure measured at the inlet, midpoint and at exit during the three cases mentioned above. For the inviscid flow of the Fluid-1 which are shown by dotted blue lines, the pulse propagates without any loss in amplitude in the absence of any damping effects viz., viscous force, reflections. During the first case of viscous flow (case ii) which are shown by solid green

lines, the propagating pulse gets progressively attenuated due to the viscous effects and there is a drop of 3.5% in amplitude along the domain length. During the second case of viscous flow (case iii) which are shown by dashed red lines, the pulse propagates at a faster speed as expected due to smaller viscous effect, there is a negligible change in the amplitude of the pressure wave along the length, which is approximately 0.06%.

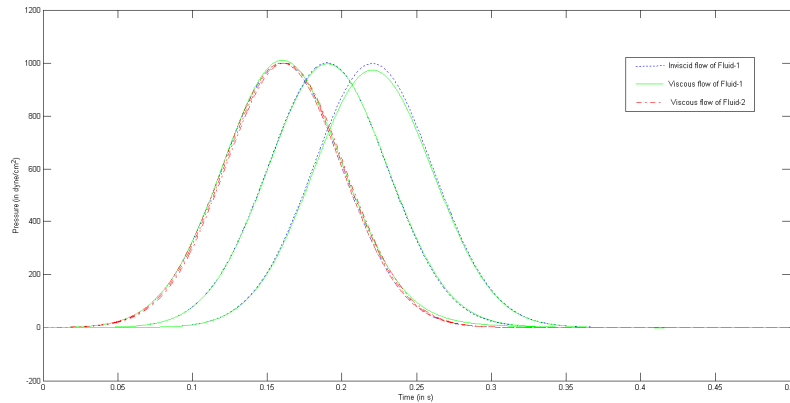


Figure 3.1 (a) – Pulse propagation through a single vessel (dotted line, solid line and dashed line represent inviscid flow, first viscous flow case and second viscous flow case respectively)

Figure 3.1 (b) shows the deformation plot of the vessel for the first viscous flow case (case ii) and the contours indicate the change in the pressure. The yaxis represent the length of the segment.

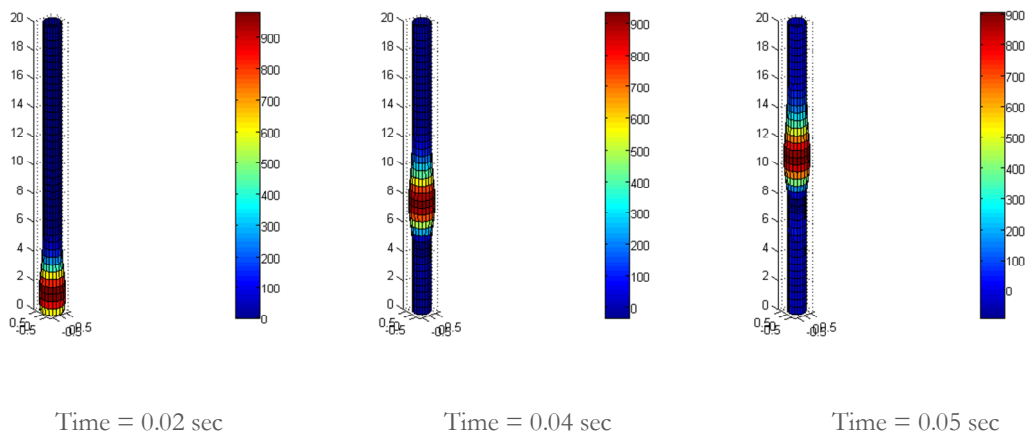


Figure 3.1 (b) - Deformation (magnified 100 times) of the vessel with pressure intensities at time 0.02s, 0.04s, 0.05s during the first viscous flow case (case ii)

## 3.2 DISCONTINUITIES

In this section, the effect of discontinuities in the network model that arise due to the changes in the cross sectional area,  $A_0$  and material parameter,  $\beta$  on the passing pressure wave is demonstrated. The details of the model used is shown in figure 3.2. These discontinuities as discussed earlier will give rise to reflections in the flow. Figure 3.3 (a) & (b) show the effect of sudden changes in the cross sectional area in a vessel segment and Figure 3.4 (a) & (b) show the effect of sudden changes in the material parameter,  $\beta$ . For all these cases, the flow is assumed to have a dynamic viscosity of 0.035 P and density 1.06 g/cm<sup>3</sup>.

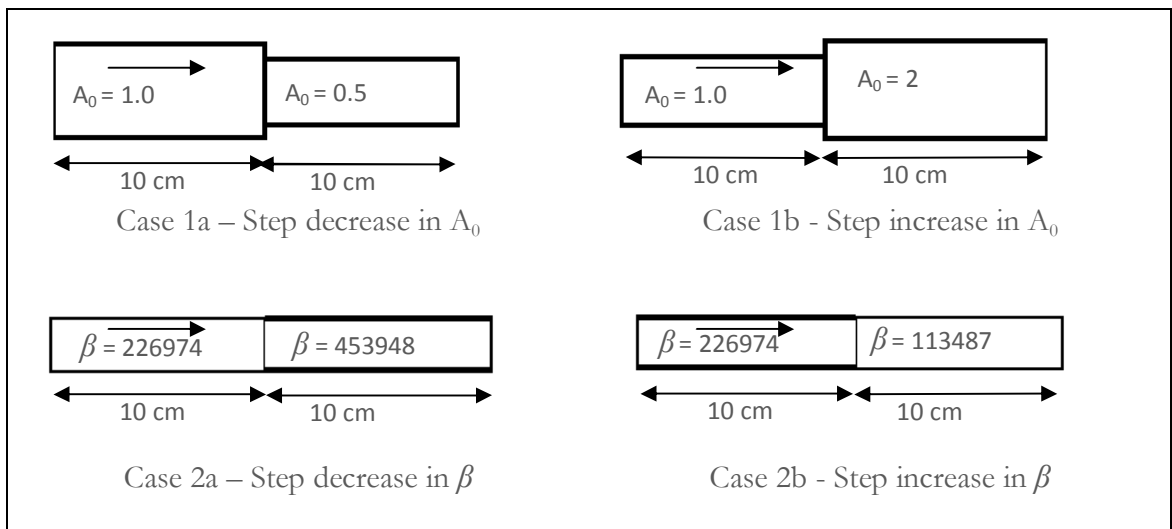


Figure 3.2 – Models used to study the discontinuities arising due to  $A_0$  and  $\beta$

It can be seen from Figure 3.3 (a) that a sudden constriction in the vessel, represented by a step decrease in the cross-sectional area,  $A_0$  value from 1.0 cm<sup>2</sup> to 0.5 cm<sup>2</sup>, results in an increase in the characteristic impedance causing a positive reflection of a portion of the transmitted wave. It can be computed from Eq. 2.5 that the linear reflection coefficient for this case is  $R_t = 0.254$ . Conversely, Figure 3.3 (b) shows that a sudden dilation of the vessel, represented by a step increase in the cross-sectional area,  $A_0$  value from 1.0 cm<sup>2</sup> to 2.0 cm<sup>2</sup>, results in a decrease in the characteristic impedance and hence the negative  $R_t = -0.254$  causes a negative reflection of a portion of the transmitted wave. Also, in the lower airways, the vessel segments progressively become narrower and shorter down from the Trachea with only a few exceptions until it reaches the respiratory airways and hence there are more likely to be partial positive reflections.

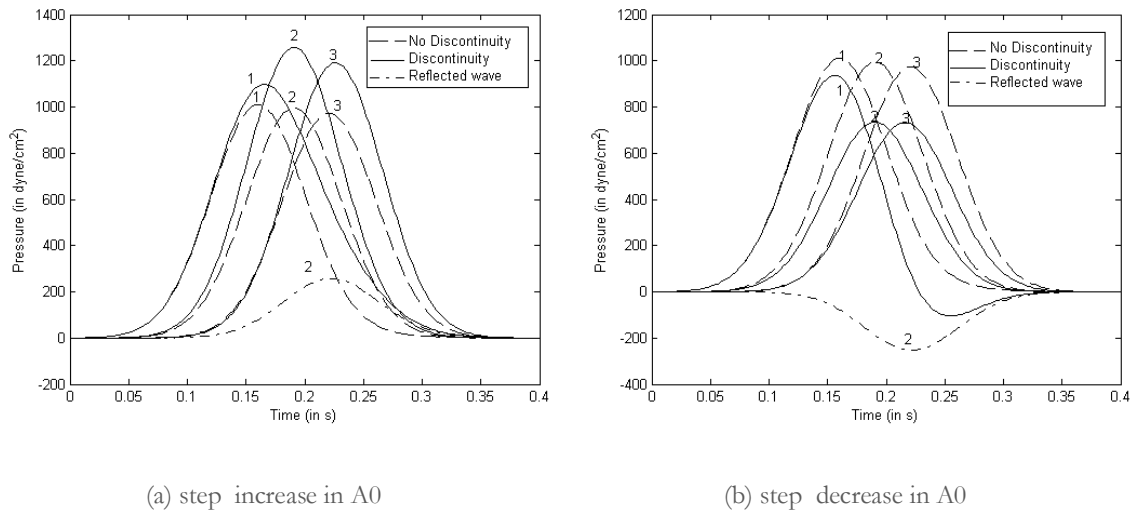


Figure 3.3 – Effect of sudden change in cross-sectional area in a single vessel

[Note: Numbers next to the plot series indicate the monitoring positions, 1-inlet, 2- start of discontinuity, 3-exit]

It can be seen from Figure 3.4 (a) that a increase in the stiffness of the vessel, represented by a step increase in the material parameter,  $\beta$  value from 226974 dyne/cm<sup>3</sup> to 453948 dyne/cm<sup>3</sup>, results in an increase in the characteristic impedance causing a positive reflection of a portion of the transmitted wave. The linear reflection coefficient for this case was found to be  $R_t = 0.171$ . On the other hand, Figure 3.4 (b) shows that a sudden softening of the vessel, represented by a step decrease in the  $\beta$  value from 226974 dyne/cm<sup>3</sup> to 113487 dyne/cm<sup>3</sup>, results in a negative reflection coefficient,  $R_t = -0.171$  causing a negative reflection of a portion of the transmitted wave. It should also be noted from Eq. 2.16a that increase in  $\beta$  will also increase the wave speed,  $c$  (as  $c \propto \beta^{1/2}$ ). Interestingly, the latter case is identical to what happens in the respiratory zone of the airways where the tissues become softer to achieve the enormous change in volume in the alveoli where the velocity of flow drops down entirely.



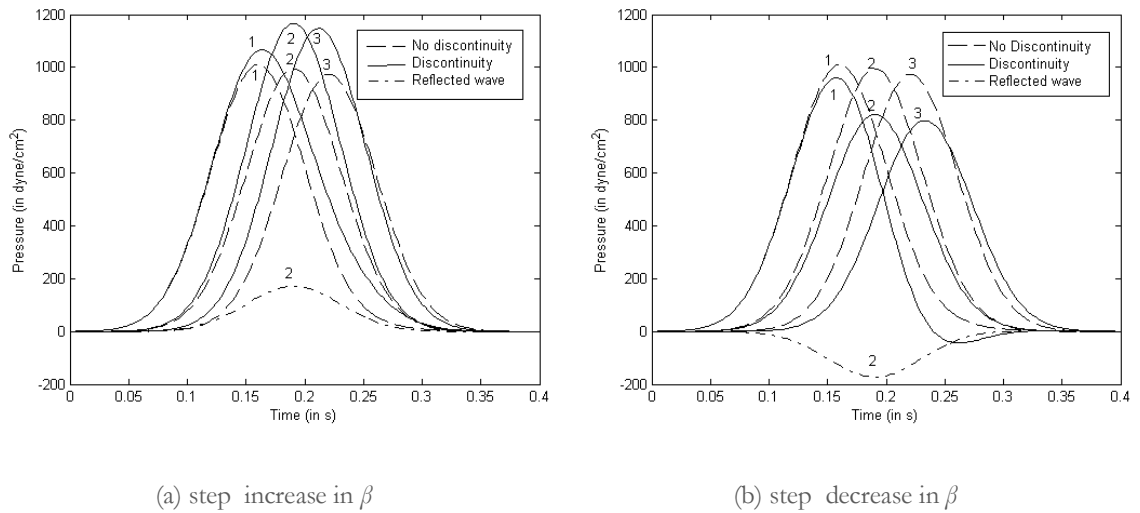


Figure 3.4 – Effect of sudden change in material properties ( $\beta$  value) in a single vessel

[Note: Numbers next to the plot series indicate the monitoring positions, 1-inlet, 2- start of discontinuity, 3-exit]

### 3.3 BRANCHING VESSELS

In airways, whenever the parent airways branch into the daughter airways it gives rise to reflection and re-reflection of the transmitted wave. In this section, the effects of branching on the flow are discussed by means of a model problem. The model used for the study is shown in Figure 3.5. The properties of the vessel are: for vessel A,  $A_0=4 \text{ cm}^2$ ,  $l= 10 \text{ cm}$ ,  $\beta = 113487 \text{ dyne/cm}^3$ , for vessel B,  $A_0=0.5 \text{ cm}^2$ ,  $l= 5 \text{ cm}$ ,  $\beta = 453948 \text{ dyne/cm}^3$ , for vessel C,  $A_0 =0.35 \text{ cm}^2$ ,  $l= 10 \text{ cm}$ ,  $\beta = 226974 \text{ dyne/cm}^3$ .

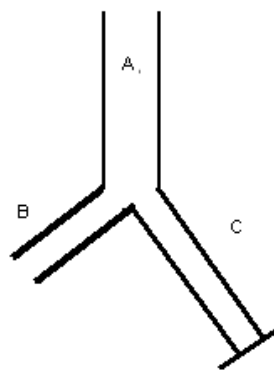


Figure 3.5 – Model of branching airways

It can be seen from Figure 3.6 the occurrence of reflections of the transmitted wave in the airway branches. The top, middle and bottom plots show the pressure monitored in the midpoint of the vessel A, B and C respectively. As the wave traverses through A and

reaches the branching point, the first backward wave into A occurs. The increase in pressure is observed in the other two vessels due to the sudden decrease in cross sectional area and due to mass conservation. The next reflection occurs at the end of the vessel C due to a imposed reflection coefficient,  $R_t = 1$  which results in the positive reflection of the wave. When this wave reaches the branching point, a negative backward wave originates back into C and rest of it is transmitted into A and B depending on their reflection coefficients and observing the continuity criteria. This reflection of waves continues until either they exit the model or damped out by the viscous terms.

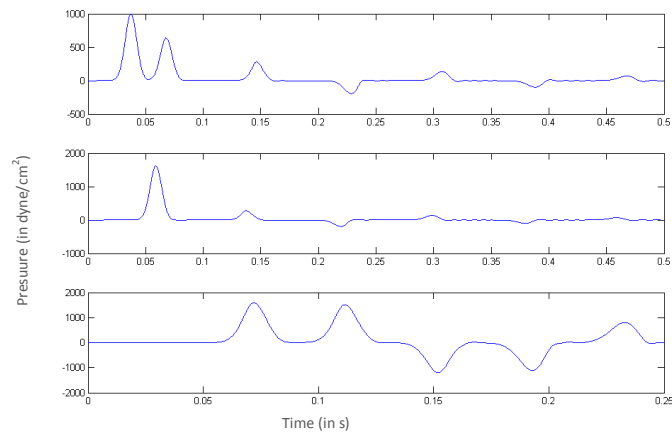


Figure 3.6 – Propagation of pulse through model 1 showing the occurrence of reflections and re-reflections

### 3.4 Formaggia model

This is a simple model of a single vessel used by Formaggia [2001] with the properties  $l = 6$  cm,  $A_0 = 0.7854$  cm<sup>2</sup> and  $\beta = 186000$  dyne/cm<sup>3</sup>. The fluid has a density,  $\rho = 1$  g/cm<sup>3</sup> and viscosity,  $\mu = 0.0350$  P. The input pressure wave has a peak amplitude of 20000 dyne/cm<sup>2</sup> with a wave speed of approximately 290 cm/s and a frequency of 0.04 s. Figure 3.6 shows the 3D representation of the deformation of the vessel at various time instances of 0.02 s, 0.03 s and 0.04 s magnified by a scaling factor of 5 and the contours indicate the mean pressure values measured along the segment.

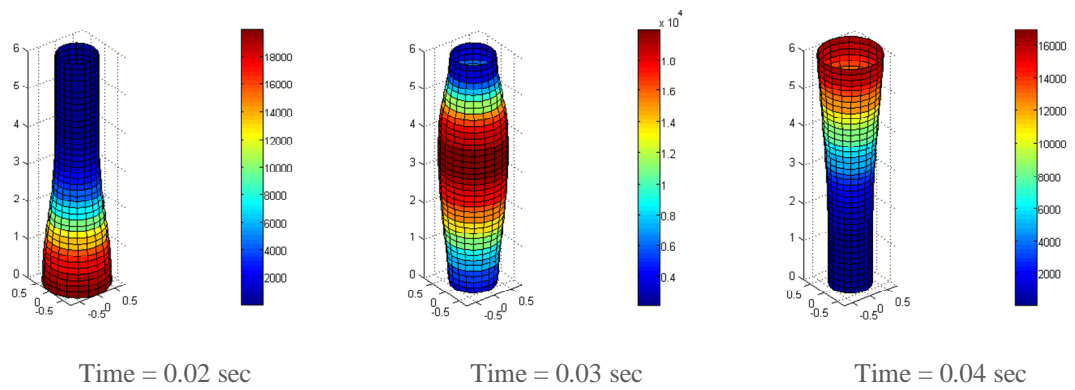


Figure 3.6 - Deformation (magnified 5 times) of the vessel with pressure intensities at time 0.02 s, 0.03 s, 0.04 s

# CHAPTER 4

## RESULTS AND DISCUSSIONS

### 4.1 INTRODUCTION

In this chapter, the results obtained from studying the fluid (air) flow through the human lower airways are presented. For this purpose, the geometric data provided by Weibel *et al.* and Horsfield *et al.* have been used. Firstly, section 4.2 demonstrates the flow of a wave representing the inspiration phase through various generation models. This will demonstrate the influence of reflecting waves due to discontinuities on the transmitted wave as the model is evolved from a simple first generation model to a 10<sup>th</sup> generation model with 2047 segments based on Weibel model. In section 4.3, a 10<sup>th</sup> generation Horsfield model is demonstrated to highlight the influence of unsymmetric branching order on the fluid flow. In section 4.4, single path models are demonstrated and their drawbacks are highlighted. In section 4.5, the effect of volume changes on the flow velocity is shown. Finally, in section 4.6, some sample cases of obstructed airways are demonstrated to show its influence on airflow distribution through the pathways.

### 4.2 WEIBEL MODEL

In this section, the lung models are constructed based on the geometric details published by Weibel [Weibel 1963]. Table 1 gives the geometric details of the Weibel model used in the test cases done in this section. It should be noted from the Figure 4.1 that the greatest increase in branching occurs beyond the 16<sup>th</sup> generation. Figure 4.2 shows the pressure wave form applied at the inlet of the Trachea producing a peak flow rate of 0.6 l/s with a time period of 1.6s representing the inhalation phase of the respiratory cycle. The fluid parameters unless specified otherwise are assumed to be density,  $\rho = 0.0012 \text{ g/cm}^3$  and the dynamic viscosity of the fluid,  $\mu = 1.824 \times 10^{-4} \text{ P}$ . These represent the properties of air at 20°C. Here, generation represent each stages of airway bifurcation. The material characteristics of the airways vary considerably with each generations as discussed earlier.

Since the upper airways are made of cartilages and are stiffer, these segments are modelled with a sufficiently large  $\beta$  value. In addition, adoption the stiffer segments helps us to identify the changes in the flow properties due to the changes in the geometric properties of the vessels only (eg., vessel constriction, vessel obstruction, etc.).

Table 4.1 – Geometric details of the Weibel model

<b>Generation</b>	<b>No. per generation</b>	<b>Diameter (in cm)</b>	<b>Length (in cm)</b>	<b>Total volume (in cm<sup>3</sup>)</b>	<b>Total cross-sectional area (in cm<sup>2</sup>)</b>
0	1	1.8	12	30.52	2.54
1	2	1.22	4.76	11.12	2.34
2	4	0.83	1.9	4.11	2.16
3	8	0.56	0.76	1.50	1.97
4	16	0.45	1.27	3.23	2.54
5	32	0.35	1.07	3.29	3.08
6	64	0.28	0.9	3.54	3.94
7	128	0.23	0.76	4.04	5.32
8	256	0.186	0.64	4.45	6.95
9	512	0.154	0.54	5.15	9.53
10	1024	0.13	0.46	6.25	13.58
11	2048	0.109	0.39	7.45	19.10
12	4096	0.095	0.33	9.58	29.02
13	8192	0.082	0.27	11.67	43.24
14	16384	0.074	0.23	16.20	70.43
15	32768	0.066	0.2	22.41	112.05
16	65536	0.06	0.165	30.56	185.20
17	131072	0.054	0.141	42.30	300.03
18	262144	0.05	0.117	60.19	514.46
19	524288	0.047	0.099	90.01	909.15
20	1048576	0.045	0.083	138.35	1666.84
21	2097152	0.043	0.07	213.08	3043.94
22	4194304	-	-	-	-
23	8388608	-	-	-	-

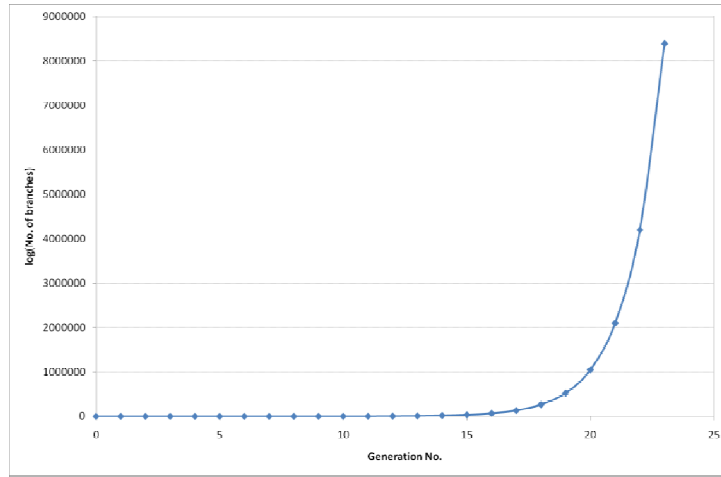


Figure 4.1 – Number of branching at each generation

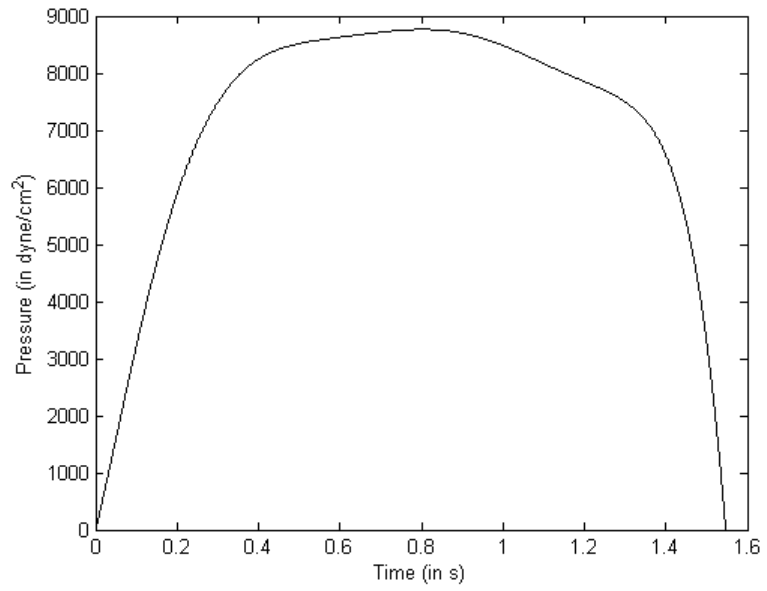


Figure 4.2 – Input pressure waveform

### 4.2.1 ONE GENERATION WEIBEL MODEL

In this case, a single vessel segment with a length of 12 cm,  $A_0 = 2.545 \text{ cm}^2$  and  $\beta = 1000000 \text{ dyne/cm}^3$  is considered. The geometric properties represent that of the Trachea and high  $\beta$  value was assumed to represent a stiffer vessel as the Trachea is lined with C-shaped cartilages.

Figure 4.3 (a) and 4.3 (b) shows the velocity and pressure measurements monitored at the mid-length of the vessel segment. It can be noted that the intrinsic wave speed calculated for this section was  $c_0 = 2578 \text{ cm/s}$ . The time step size adopted was  $dt = 4 \times 10^{-4} \text{ s}$  and a uniform mesh size of 1.2 cm. In the absence of any discontinuity and the only damping is offered by the viscosity.

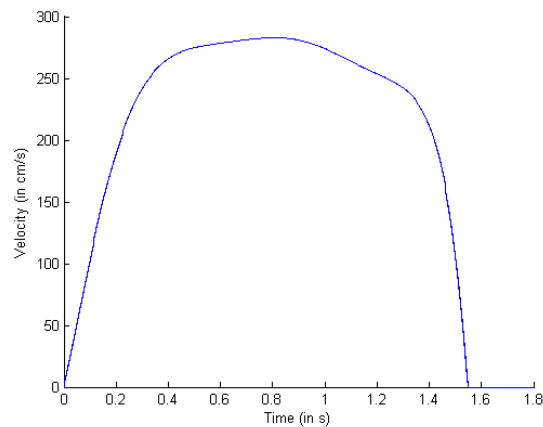


Figure 4.3 (a) – Velocity measurement in the Generation-1 model plotted against time

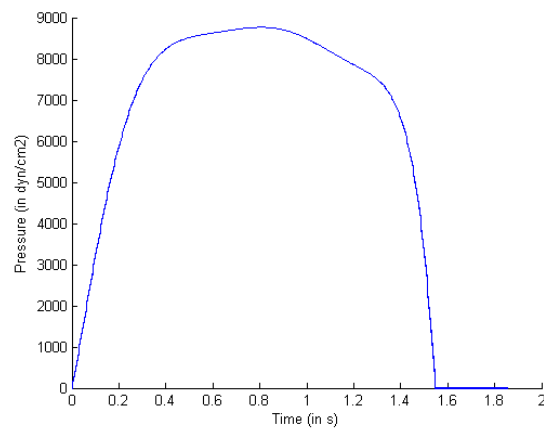


Figure 4.3 (b) – Pressure measurement in the Generation-1 model plotted against time

### 4.2.2 TWO GENERATION WEIBEL MODEL

In this case, a two generation model with three airway segments comprising of a parent vessel and two daughter vessels. The parent vessel is with a length of 12 cm,  $A_0 = 2.545 \text{ cm}^2$  and  $\beta = 1000000 \text{ dyne/cm}^3$  and both the daughters have a length of 4.76 cm,  $A_0 = 1.169 \text{ cm}^2$  and  $\beta = 1000000 \text{ dyne/cm}^3$  is considered. The geometric properties represent that of the Trachea and primary bronchi.

Figure 4.4 (a) shows the nodal arrangement for this model. Figure 4.4 (b) and 4.4 (c) shows the velocity and pressure measurements monitored at the mid-length of the vessel segments. It can be noted that the intrinsic wave speed at inlet calculated for this section was  $c_0 = 2578 \text{ cm/s}$ . The time step size adopted was  $dt = 1 \times 10^{-5} \text{ s}$  and a uniform mesh size of  $L/10$ . Due to the presence of branching, a drop in the pressure value can be observed due to a negative reflection arising due to vessel branching and section narrowing as discussed in Chapter 3. The velocity computed in the daughter segment has increased due to the decrease in cross-sectional area as expected. It shall be seen that velocity will keep increasing until the flow crosses 5<sup>th</sup> to 6<sup>th</sup> generation beyond which it will start to drop due to increase in the total cross sectional area at that generation.

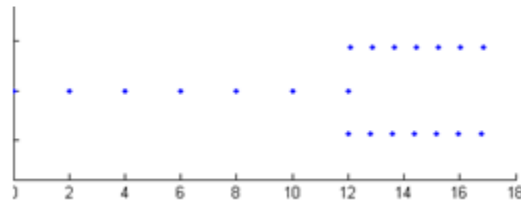


Figure 4.4 (a) – Nodal positions for the Generation-2 model

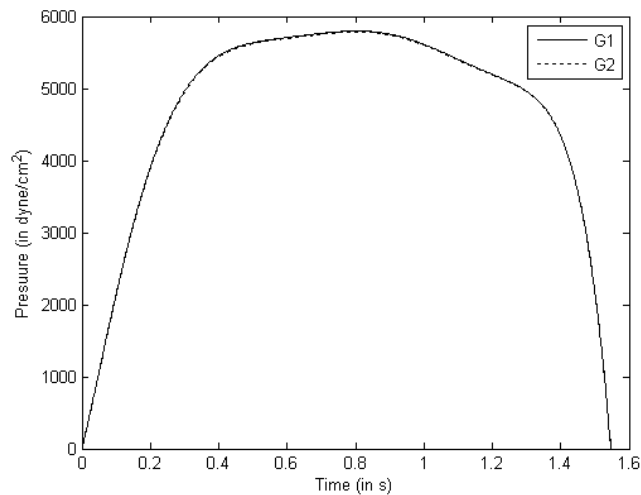


Figure 4.4 (b) – Velocity measurement in the Generation-2 model plotted against time



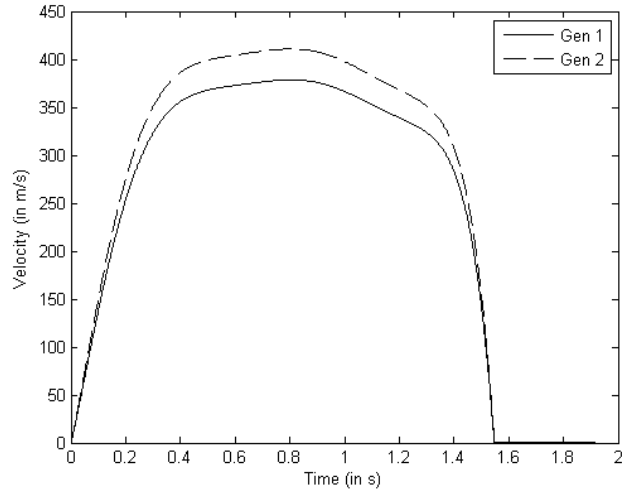


Figure 4.4 (c) – Pressure measurement in the Generation-2 model plotted against time

### 4.2.3 THREE GENERATION WEIBEL MODEL

In this case, a three generation model with seven airway segments is considered. The vessel in the first generation has a length of 12 cm,  $A_0 = 2.545 \text{ cm}^2$  and  $\beta = 1000000 \text{ dyne/cm}^3$ , segments in the second generation have a length of 4.76 cm,  $A_0 = 1.169 \text{ cm}^2$  and  $\beta = 1000000 \text{ dyne/cm}^3$  and the segments in the third generation have a length of 1.9 cm,  $A_0 = 0.541 \text{ cm}^2$  and  $\beta = 1000000 \text{ dyne/cm}^3$ . The geometric properties represent that of the Trachea, primary bronchi and secondary bronchi.

Figure 4.5 (a) shows the nodal arrangement for this model. Figure 4.5 (b) and 4.5 (c) shows the velocity and pressure measurements monitored at the mid-length of the vessel segments. It can be noted that the intrinsic wave speed at inlet calculated for this section was  $c_0 = 2578 \text{ cm/s}$ . The time step size adopted was  $dt = 5 \times 10^{-6} \text{ s}$  and a uniform mesh size of  $L/10$ . Due to the presence of branching, drop in the pressure value can be observed due to a negative reflection arising due to vessel branching and section narrowing as discussed earlier. The velocity computed increases as the flow passes down the airways due to the decrease in cross-sectional area.

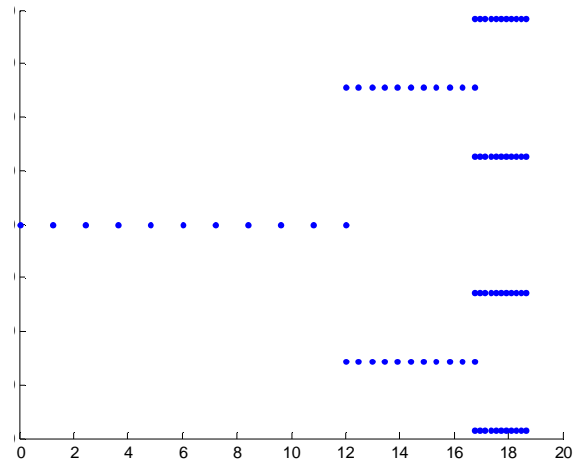


Figure 4.5 (a) – Nodal positions for the Generation-3 model

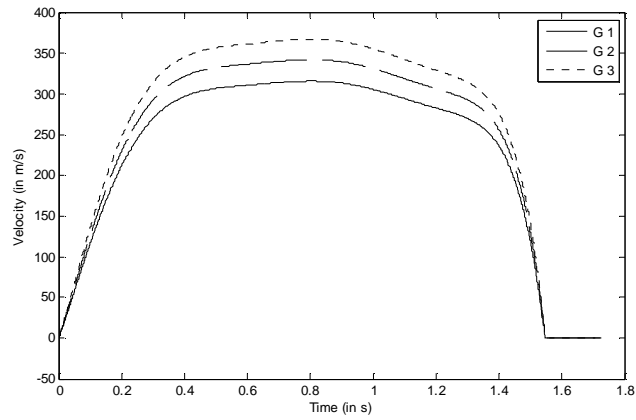


Figure 4.5 (b) – Velocity measurement in the Generation-3 model plotted against time

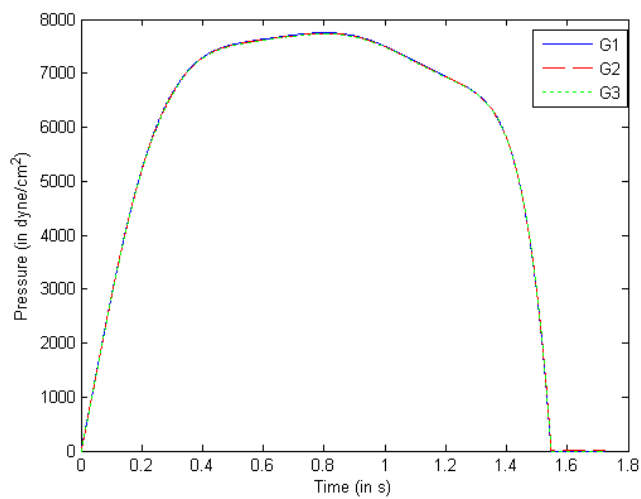


Figure 4.5 (c) – Pressure measurement in the Generation-3 model plotted against time

#### 4.2.4 FOUR GENERATION WEIBEL MODEL

In this case, a four generation model with 15 airway segments is considered. The vessel properties are given in Table 4.2.

Table 4.2 – Properties of the vessel segment

Generation	No. per generation	Diameter (in cm)	Area (in cm <sup>2</sup> )	Length (in cm)	$\beta$ (dynes/cm <sup>3</sup> )
1	1	1.8	2.54	12	1000000
2	2	1.22	1.17	4.76	1000000
3	4	0.83	0.54	1.9	1000000
4	8	0.56	0.76	0.76	1000000

Figure 4.6 (a) shows the nodal arrangement for this model. Figure 4.5 (b) and 4.5 (c) shows the velocity and pressure measurements monitored at the mid-length of the vessel segments. It can be noted that the intrinsic wave speed at inlet calculated for this section was  $c_0 = 2577$  cm/s. The time step size adopted was  $dt = 5 \times 10^{-6}$  s and a uniform mesh size of  $L/10$ . The variation in pressure and velocity follows the same trend as earlier.

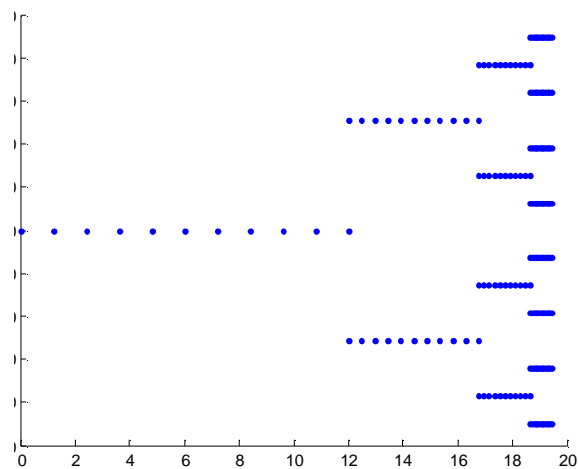


Figure 4.6 (a) – Nodal positions for the Generation-4 model

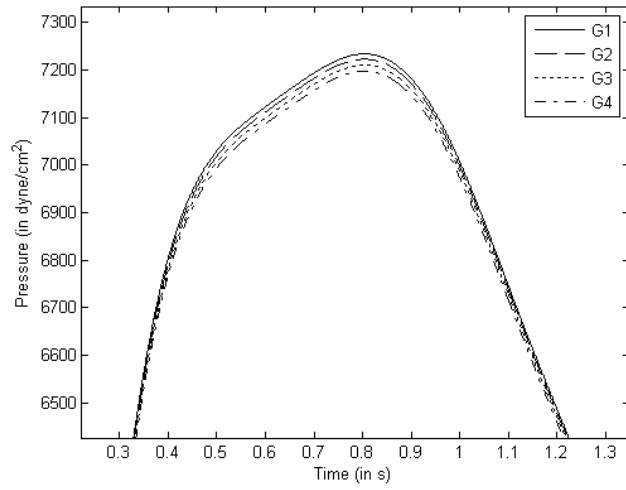


Figure 4.6 (b) – Pressure measurement in the Generation-4 model plotted against time

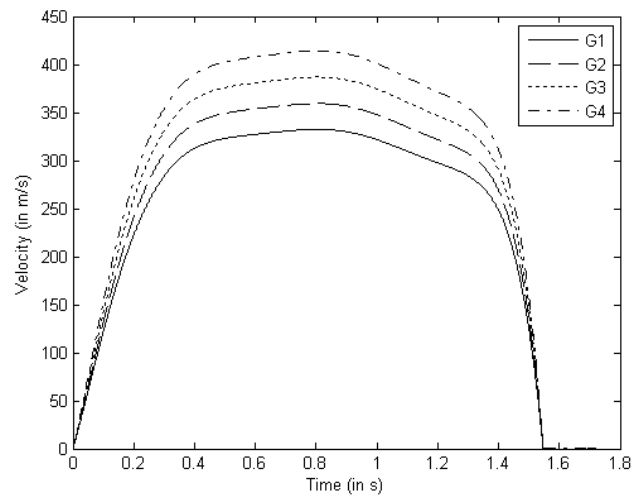


Figure 4.6 (c) – Velocity measurement in the Generation-4 model plotted against time

### 4.2.5 FIVE GENERATION WEIBEL MODEL

In this case, a five generation model with 31 airway segments is considered. The vessel properties are given in Table 4.3.

Table 4.3 – Properties of the vessel segment

Generation	No. per generation	Diameter (in cm)	Area (in cm <sup>2</sup> )	Length (in cm)	$\beta$ (dynes/cm <sup>3</sup> )
1	1	1.8	2.54	12	1000000
2	2	1.22	1.17	4.76	1000000
3	4	0.83	0.54	1.9	1000000
4	8	0.56	0.25	0.76	1000000
5	16	0.45	0.16	1.27	1000000

Figure 4.7 (a) shows the nodal arrangement for this model. Figure 4.7 (b) and 4.7 (c) shows the velocity and pressure measurements monitored at the mid-length of the vessel segments. It can be noted that the intrinsic wave speed at inlet calculated for this section was  $c_0 = 2577$  cm/s. The time step size adopted was  $dt = 5 \times 10^{-6}$  s and a uniform mesh size of  $L/10$ . Due to the presence of branching, drop in the pressure value can be observed due to a negative reflection arising due to vessel branching and section narrowing as discussed earlier. The velocity computed increases as the flow passes down the airways due to the decrease in cross-sectional area.

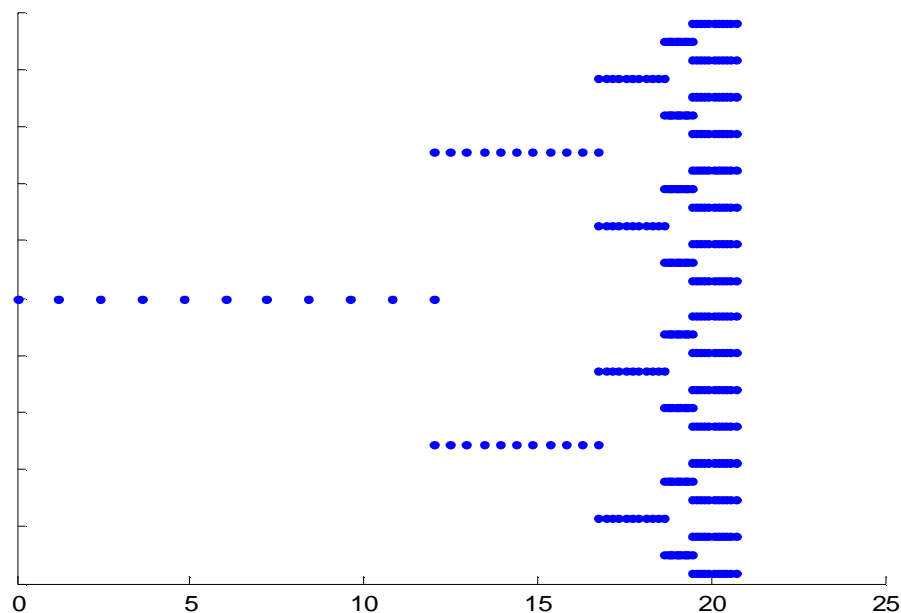


Figure 4.7 (a) – Nodal positions for the Generation-5 model

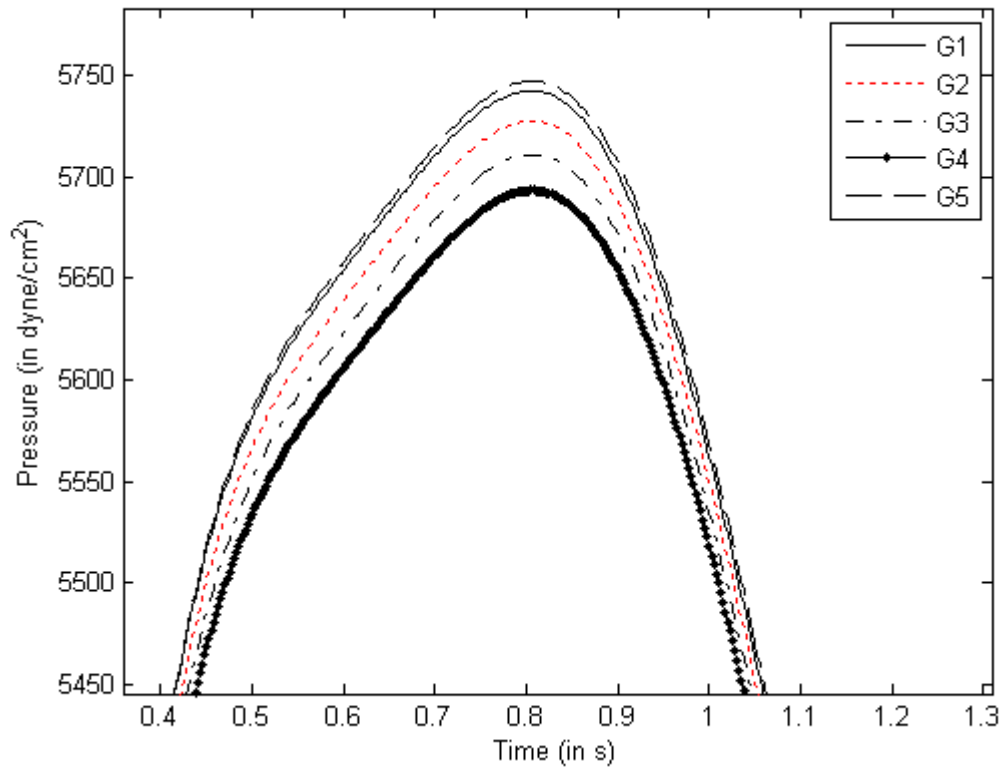


Figure 4.7 (b) – Pressure measurement in the Generation-5 model plotted against time

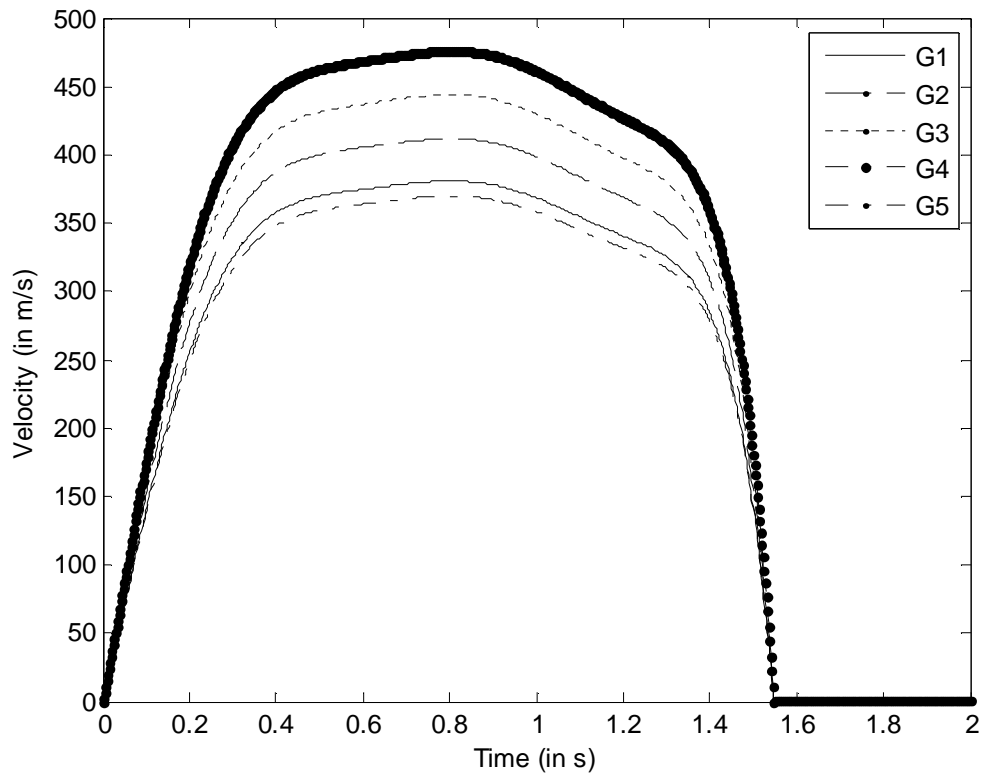


Figure 4.7 (c) – Velocity measurement in the Generation-5 model plotted against time

#### 4.2.6 SIX GENERATION WEIBEL MODEL

In this case, a six generation model with 63 airway segments is considered. The vessel properties are given in Table 4.4. Figure 4.8 (a) shows the nodal points of this model. Figure 4.8 (b) and 4.8 (c) shows the velocity and pressure measurements monitored at the mid-length of the vessel segments. It can be noted that the intrinsic wave speed at inlet calculated for this section was  $c_0 = 2577$  cm/s. The time step size adopted was  $dt = 5 \times 10^{-6}$  s and a uniform mesh size of  $L/10$ .

Table 4.4 – Properties of the vessel segment

Generation	No. per generation	Diameter (in cm)	Area (in cm <sup>2</sup> )	Length (in cm)	$\beta$ (dynes/cm <sup>3</sup> )
1	1	1.8	2.54	12	1000000
2	2	1.22	1.17	4.76	1000000
3	4	0.83	0.54	1.9	1000000
4	8	0.56	0.25	0.76	1000000
5	16	0.45	0.16	1.27	1000000
6	32	0.35	0.10	1.07	1000000

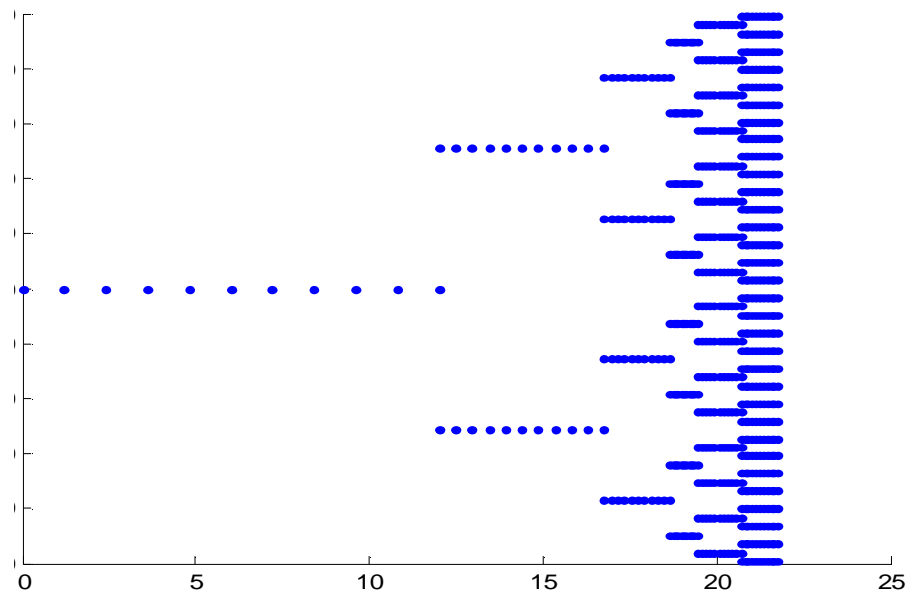


Figure 4.8 (a) – Nodal positions for the Generation-6 model

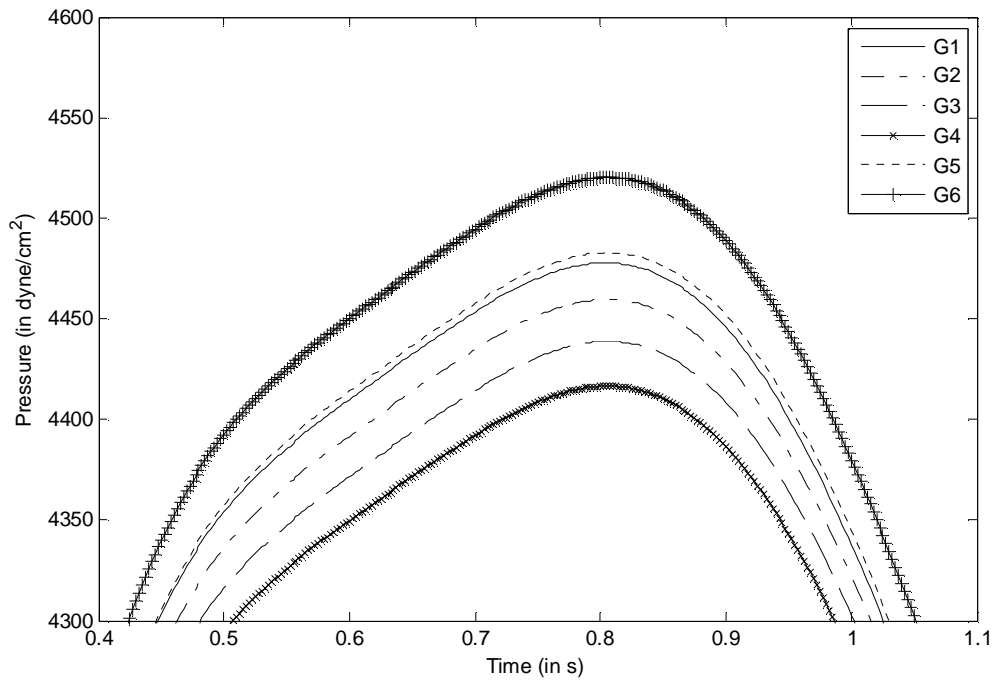


Figure 4.8 (b) – Pressure measurement in the Generation-6 model plotted against time

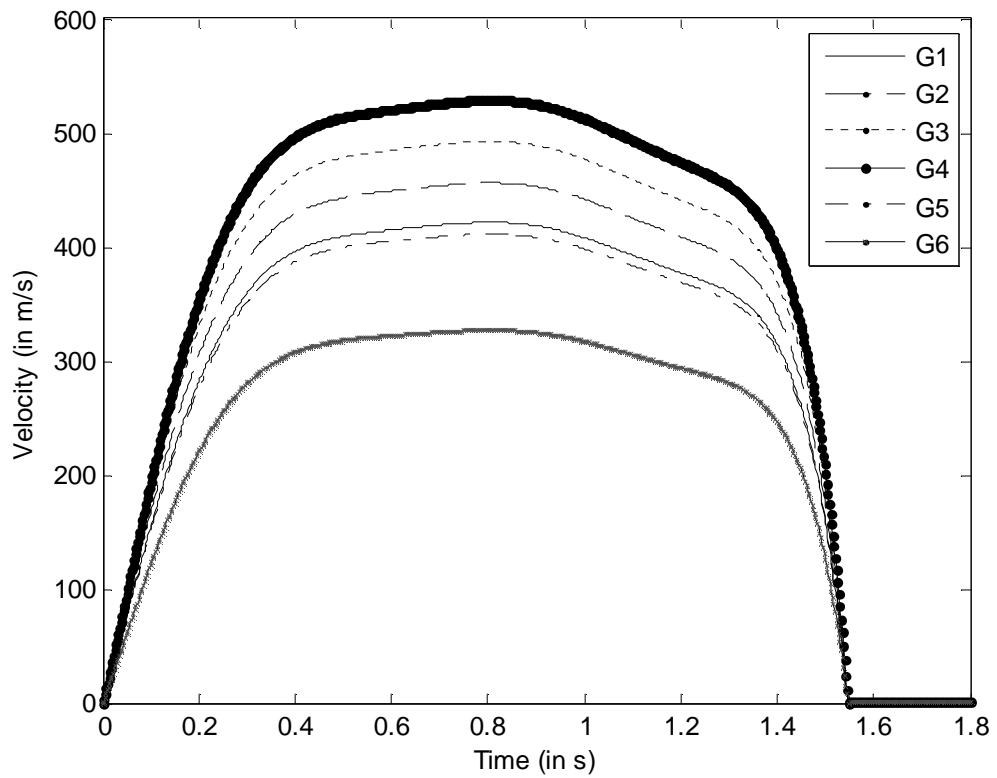


Figure 4.8 (c) – Velocity measurement in the Generation-6 model plotted against time



### 4.2.7 SEVEN GENERATION WEIBEL MODEL

In this case, a seven generation model with 127 airway segments is considered. The vessel properties are given in Table 4.5. Figure 4.9 (a) shows the nodal positions of this model. Figure 4.9 (b) and 4.9 (c) shows the velocity and pressure measurements monitored at the mid-length of the vessel segments. It can be noted that the intrinsic wave speed at inlet calculated for this section was  $c_0 = 2577$  cm/s. The time step size adopted was  $dt = 5 \times 10^{-6}$  s and a uniform mesh size of  $L/10$ .

Table 4.5 – Properties of the vessel segment

Generation	No. per generation	Diameter (in cm)	Area (in cm <sup>2</sup> )	Length (in cm)	$\beta$ (dynes/cm <sup>3</sup> )
1	1	1.8	2.54	12	1000000
2	2	1.22	1.17	4.76	1000000
3	4	0.83	0.54	1.9	1000000
4	8	0.56	0.25	0.76	1000000
5	16	0.45	0.16	1.27	1000000
6	32	0.35	0.10	1.07	1000000
7	64	0.28	0.06	0.9	1000000

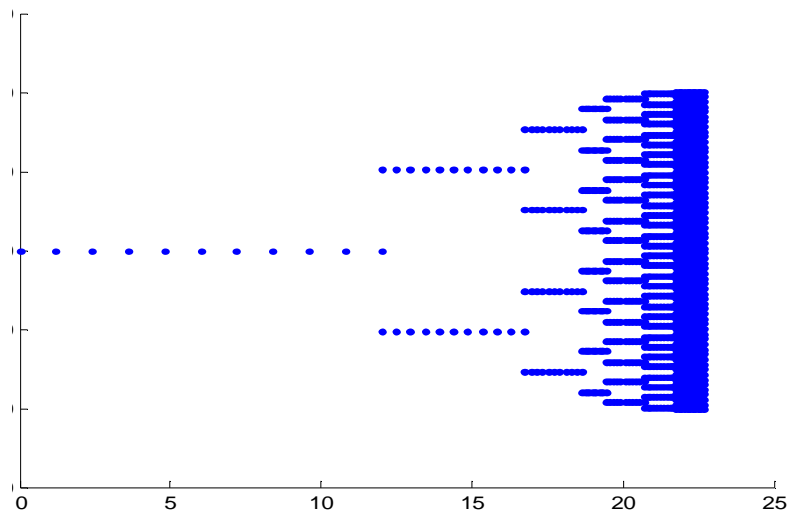


Figure 4.9 (a) – Nodal positions for the Generation-7 model

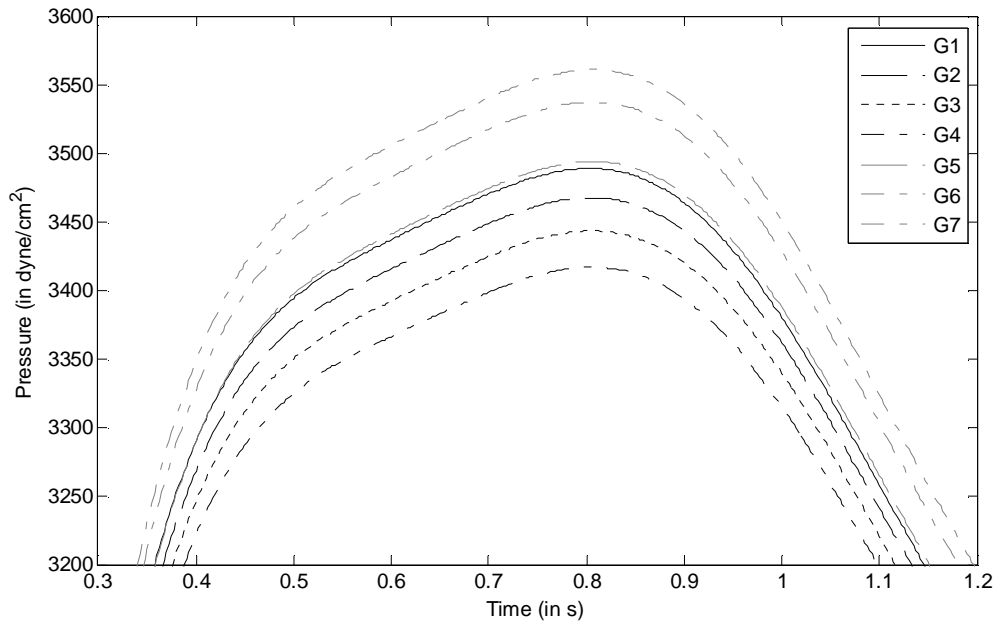


Figure 4.9 (b) – Pressure measurement in the Generation-7 model plotted against time [only a portion is shown]

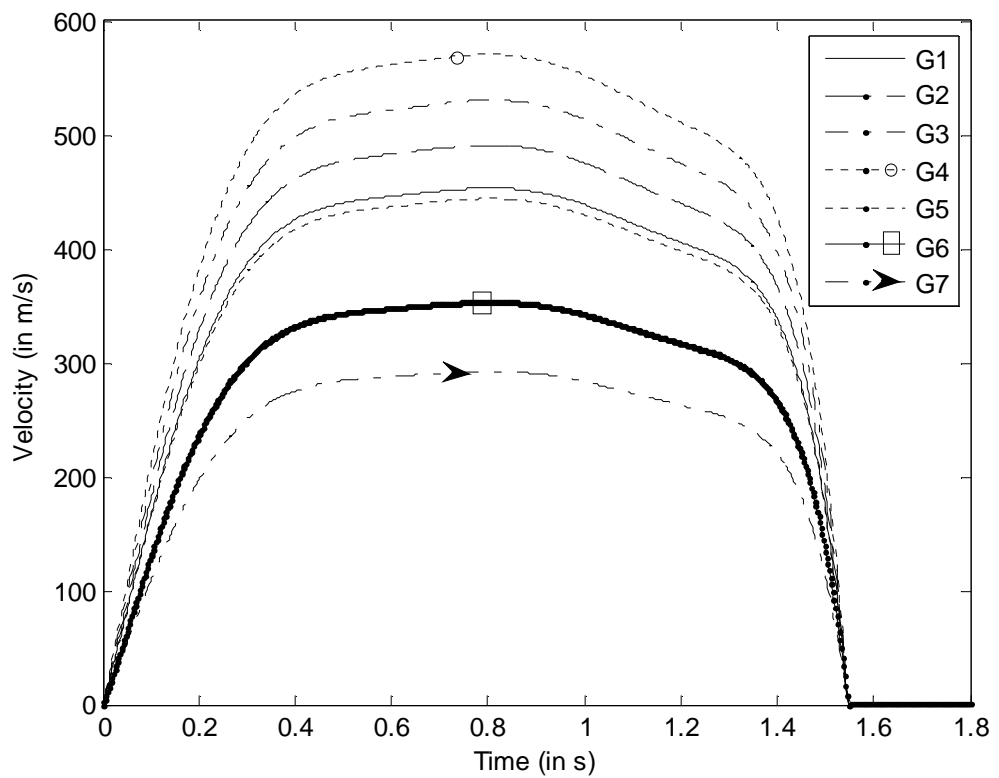


Figure 4.9 (c) – Velocity measurement in the Generation-7 model plotted against time

## 4.2.8 EIGHT GENERATION WEIBEL MODEL

In this case, a eight generation model with 255 airway segments is considered. The vessel properties are given in Table 4.6. Figure 4.10 (a) shows the nodal points of this model. Figure 4.10 (b) and 4.10 (c) shows the pressure and velocity measurements monitored at the mid-length of the vessel segments. It can be noted that the intrinsic wave speed at inlet calculated for this section was  $c_0 = 2577$  cm/s. The time step size adopted was  $dt = 5 \times 10^{-6}$  s and a uniform mesh size of  $L/10$ .

Table 4.6 – Properties of the vessel segment

Generation	No. per generation	Diameter (in cm)	Area (in cm <sup>2</sup> )	Length (in cm)	$\beta$ (dynes/cm <sup>3</sup> )
1	1	1.8	2.54	12	1000000
2	2	1.22	1.17	4.76	1000000
3	4	0.83	0.54	1.9	1000000
4	8	0.56	0.25	0.76	1000000
5	16	0.45	0.16	1.27	1000000
6	32	0.35	0.10	1.07	1000000
7	64	0.28	0.06	0.9	1000000
8	128	0.23	0.04	0.76	1000000

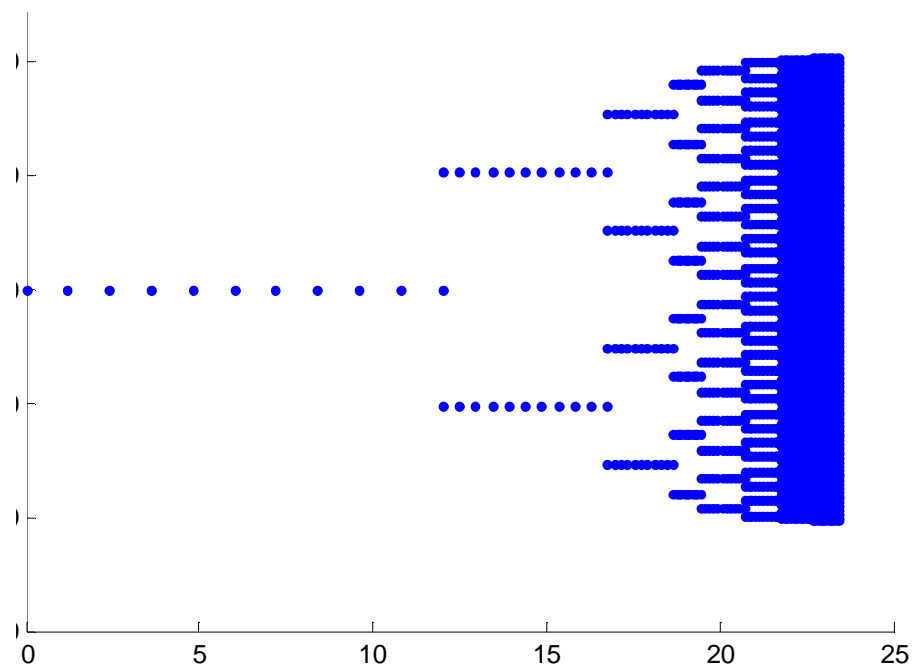


Figure 4.10 (a) – Nodal positions for the Generation-8 model

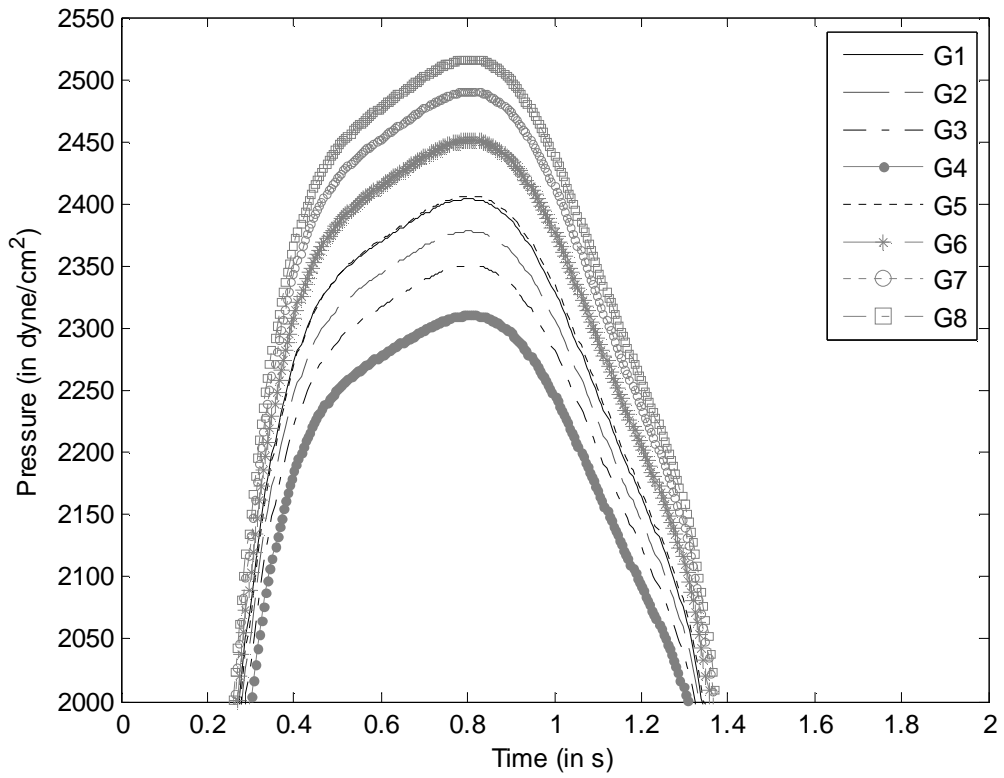


Figure 4.10 (b) – Pressure measurement in the Generation-8 model plotted against time

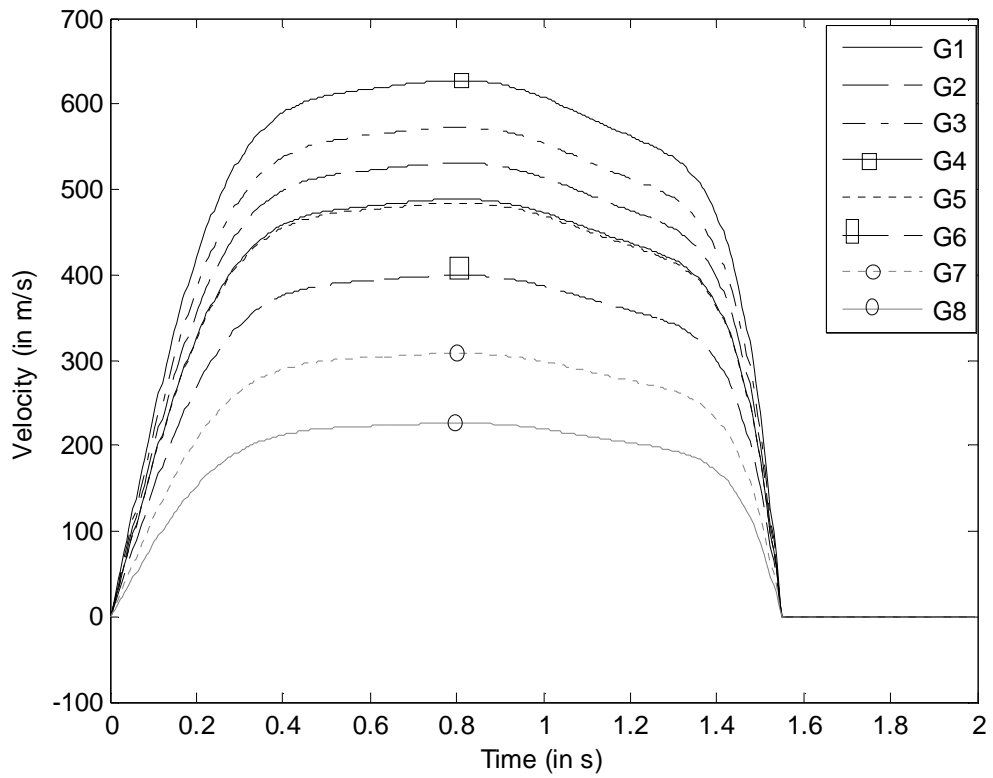


Figure 4.10 (c) – Velocity measurement in the Generation-8 model plotted against time

#### 4.2.9 NINE GENERATION WEIBEL MODEL

In this case, a nine generation model with 511 airway segments is considered. The vessel properties are given in Table 4.7. Figure 4.11 (a) shows the nodal points of this model. Figure 4.11 (b1 & b2) and 4.11 (c) shows the pressure and velocity measurements monitored at the mid-length of the vessel segments. It can be noted that the intrinsic wave speed at inlet calculated for this section was  $c_0 = 2577$  cm/s. The time step size adopted was  $dt = 5 \times 10^{-6}$ s and a uniform mesh size of  $L/10$ .

Table 4.7 – Properties of the vessel segment

Generation	No. per generation	Diameter (in cm)	Area (in cm <sup>2</sup> )	Length (in cm)	$\beta$ (dynes/cm <sup>3</sup> )
1	1	1.8	2.54	12	1000000
2	2	1.22	1.17	4.76	1000000
3	4	0.83	0.54	1.9	1000000
4	8	0.56	0.25	0.76	1000000
5	16	0.45	0.16	1.27	1000000
6	32	0.35	0.10	1.07	1000000
7	64	0.28	0.06	0.9	1000000
8	128	0.23	0.04	0.76	1000000
9	256	0.186	0.02	0.64	1000000

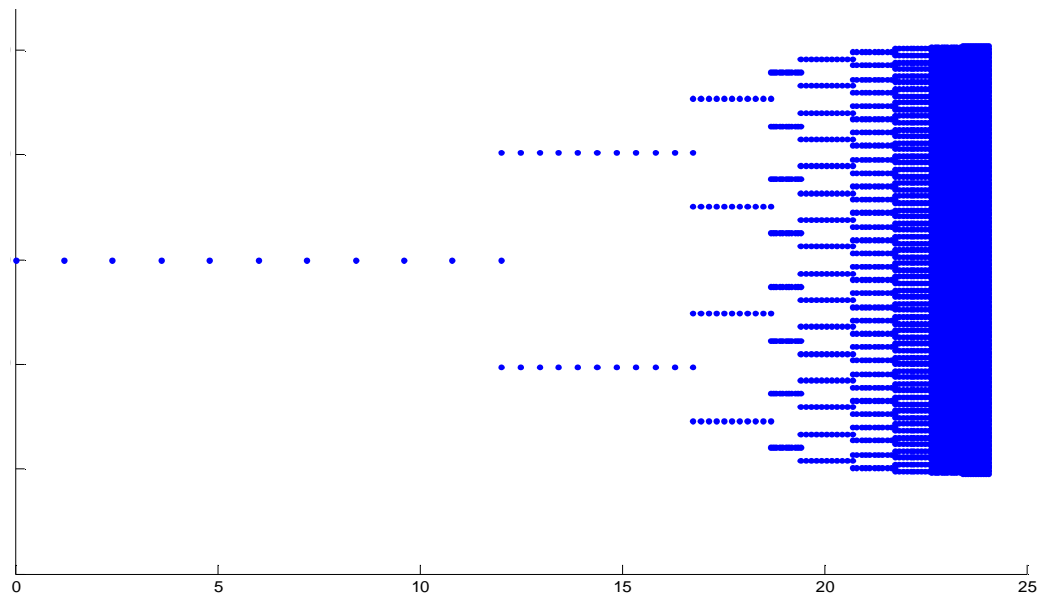


Figure 4.11 (a) – Nodal positions for the Generation-8 model

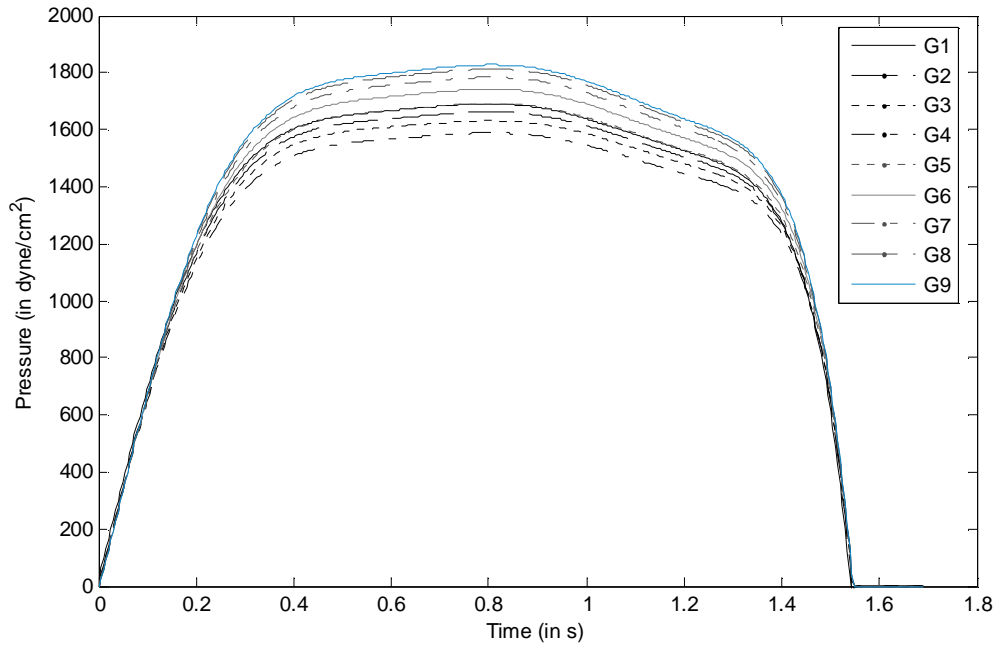


Figure 4.11 (b1) – Pressure measurement in the Generation-8 model plotted against time

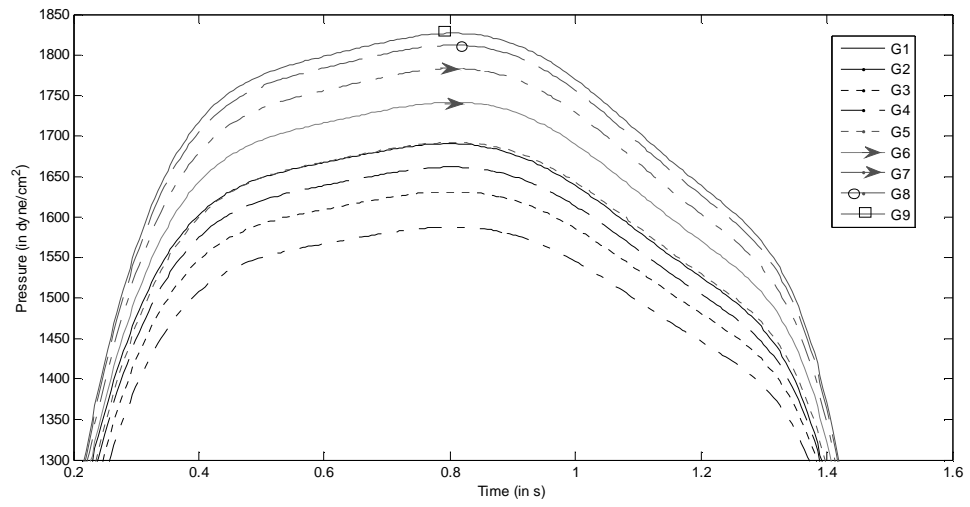


Figure 4.11 (b2) – Pressure measurement in the Generation-8 model plotted against time

[portion of Figure 4.9 (b1)]

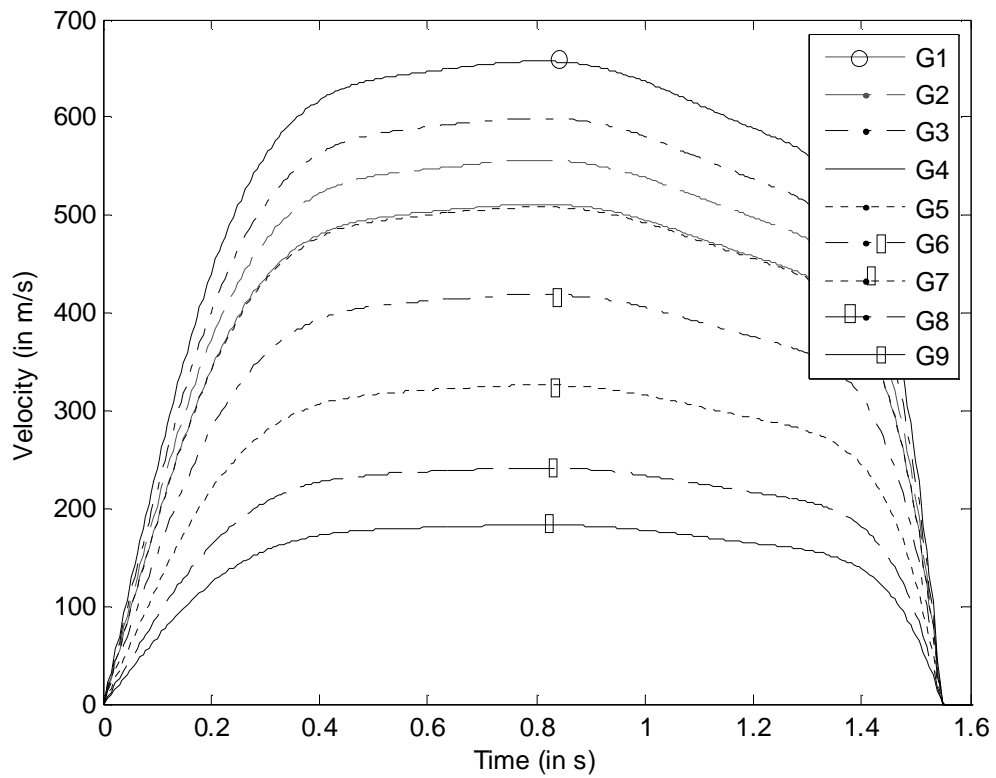


Figure 4.11 (c) – Velocity measurement in the Generation-8 model plotted against time

#### 4.2.10 SUMMARY OF THE WEIBEL MODEL

Figure 4.2.10 shows the comparison of the velocity measured against the generation no. It can be seen that initially in the upper generation there is a continuous increase in the flow velocity but beyond the 4<sup>th</sup> generation the velocity of the flow begins to drop due to the increase in the airway branching and the increase in the total cross sectional area available at each generation.

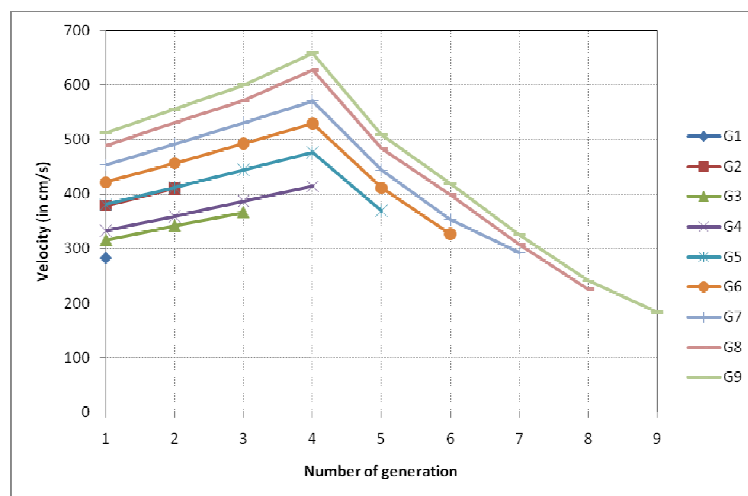


Figure 4.12– Comparison of velocity computed in the Weibel models

### 4.3 HORSFIELD MODEL

In this section, the lung models are constructed based on the geometric details published by Horsfield [Horsfield]. Table 4.7 gives the geometric details of the Horsfield model used in the test cases done in this section. It should be noted that unlike the symmetrical Weibel model, airways gives rise to unsymmetric branching. The pressure wave form shown in Figure 4.2 used for the Weibel is used here. This is applied at the inlet of the Trachea producing a peak flow rate of 0.6 l/s with a time period of 1.6s representing the inhalation phase of the respiratory cycle. The fluid parameters unless specified otherwise are assumed to be density,  $\rho = 0.0012 \text{ g/cm}^3$  and the dynamic viscosity of the fluid,  $\mu = 1.824 \times 10^{-4} \text{ P}$ . These represent the properties of air at 20°C. In Table 4.7, the branches in the same order have the same geometrical properties and are numbered starting from the terminal bronchioles to Trachea.

Table 4.7 – Airway branching details of Horsfield model 1 [H1]

Branch	Order	DB 1	DB 2	Dism, mm	Length, mm	E	Flow, % of Trachea	No. of Branches
0	31	Branch 1	Branch 10	16.0	100.00	233,920	100.0000	1
1	29	Branch 6	Branch 2	12.0	50.00	105,344	45.0342	1
2	27	Order 26	Order 23	7.5	16.00	44,256	18.9193	1
6	28	Order 27	Order 24	8.0	11.00	61,088	26.1149	1
10	30	Branch 13	Branch 11	11.1	22.00	128,576	54.9658	1
11	27	Order 26	Order 23	7.3	15.60	44,256	18.9193	1
13	29	Branch 15	Branch 14	8.9	26.00	84,320	36.0465	1
14	25	Order 24	Order 21	5.2	21.00	23,232	9.9316	1
15	28	Order 27	Order 24	6.4	8.00	61,088	26.1149	1
Bronchi within lobes	27	Order 26	Order 23	7.00	9.70	44,256	18.9193	4
	26	25	22	6.67	11.27	32,064	13.7073	4
	25	24	21	5.85	11.25	23,232	9.9316	5
	24	23	20	5.35	9.70	16,832	7.1956	7
	23	22	19	4.27	10.01	12,192	5.2120	11
	22	21	18	3.49	9.53	8,832	3.7756	15
	21	20	17	3.47	8.57	6,400	2.7360	20
	20	19	16	3.09	9.88	4,640	1.9836	27
	19	18	15	2.88	7.96	3,360	1.4364	38
	18	17	14	2.77	9.18	2,432	1.0307	53
	17	16	13	2.67	8.18	1,760	$7.5239 \times 10^{-1}$	73
	16	15	12	2.51	8.08	1,280	$5.4720 \times 10^{-1}$	99
	15	14	11	2.35	7.74	928	$3.9672 \times 10^{-1}$	138
	14	13	10	2.18	6.40	672	$2.8728 \times 10^{-1}$	191
	13	12	9	2.00	6.27	480	$2.0520 \times 10^{-1}$	262
	12	11	8	1.77	5.17	352	$1.5048 \times 10^{-1}$	364
	11	10	7	1.56	4.77	256	$1.0944 \times 10^{-1}$	501
	10	9	7	1.35	4.22	192	$8.2079 \times 10^{-2}$	690
	9	8	6	1.13	3.56	128	$5.4720 \times 10^{-2}$	957
	8	7	6	0.95	3.12	96	$4.1040 \times 10^{-2}$	1,321
	7	6	6	0.76	2.54	64	$2.7360 \times 10^{-2}$	2,516
Bronchioles	6	5	5	0.63	1.10	23	$1.3680 \times 10^{-2}$	7,310
	5	4	4	0.53	1.31	16	$6.8400 \times 10^{-3}$	14,620
	4	3	3	0.48	1.05	8	$3.4200 \times 10^{-3}$	29,240
	3	2	2	0.43	0.75	4	$1.7100 \times 10^{-3}$	58,480
	2	1	1	0.40	0.59	2	$8.5500 \times 10^{-4}$	116,960
	1			0.40	0.48	1	$4.2750 \times 10^{-4}$	233,920



### 4.3.1 EIGHT GENERATION HORSFIELD MODEL

A eight generation Horsfield model with 255 airway segments with airway sizes ranging from order-31 to order-7 of the Horsfield data shown in Table 4.7 has been performed. Figure 4.13 (a) shows the velocity measurement (in mm/s) at various segments.

Figure 4.13 (b) shows the results monitored along a selected path line covering five generation of airways. All these segments belong to a single path of branching such that the first branch belongs to the order 31 to the last one belongs to order 27. Unlike the Weibel model, it immediately becomes apparent that the airways at each generation need not have the same flow. Infact, the flow through each of the airways is uniquely defined by not only its properties and the airways above it but, the reflections arising from the lower generations will also affect the flow. It can also be seen in Figure 4.13 that the flow velocity begins to drop from the 5<sup>th</sup> generation.

Figure 4.13 (c) shows the velocity measurement through another path line (path 2). The geometric properties of the branches follow the following order 31-30-27-23-19 (these numbers correspond to the Horsfield order nos given in Table 4.7). It can be seen that the velocity increases due to the decrease in cross sectional area and after 4<sup>th</sup> generation it starts to drop.

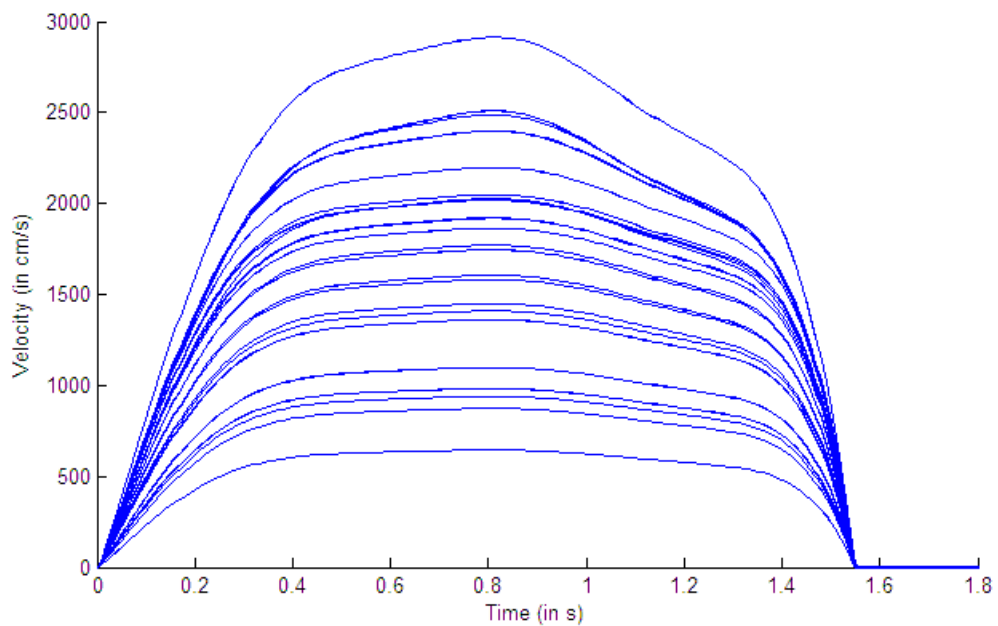


Figure 4.13 (a) – Velocity measurements across five generations

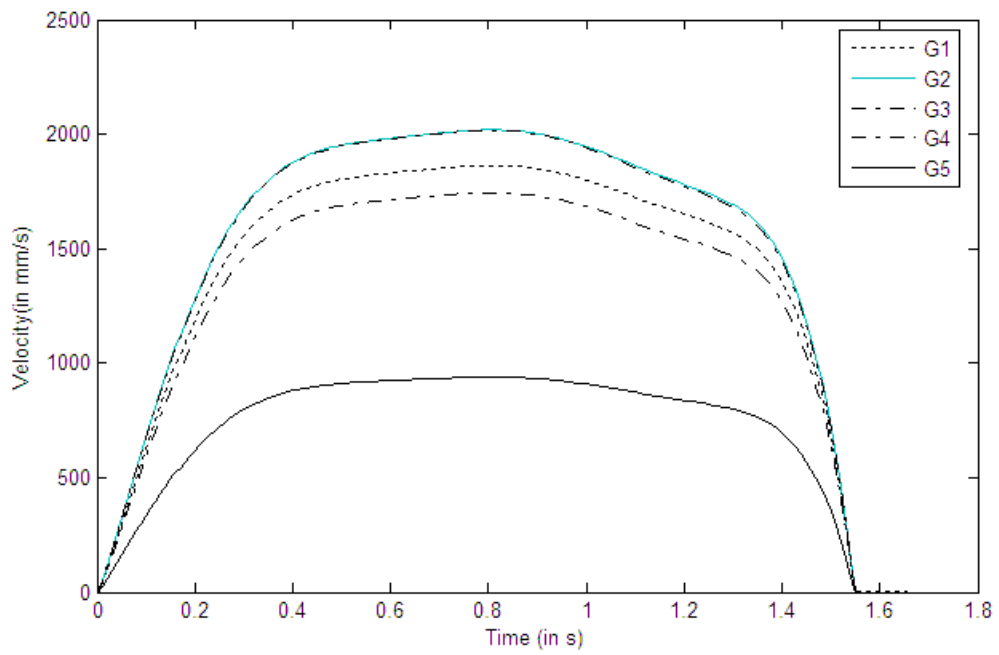


Figure 4.13 (b) – Velocity measurements across five generations (path 1)

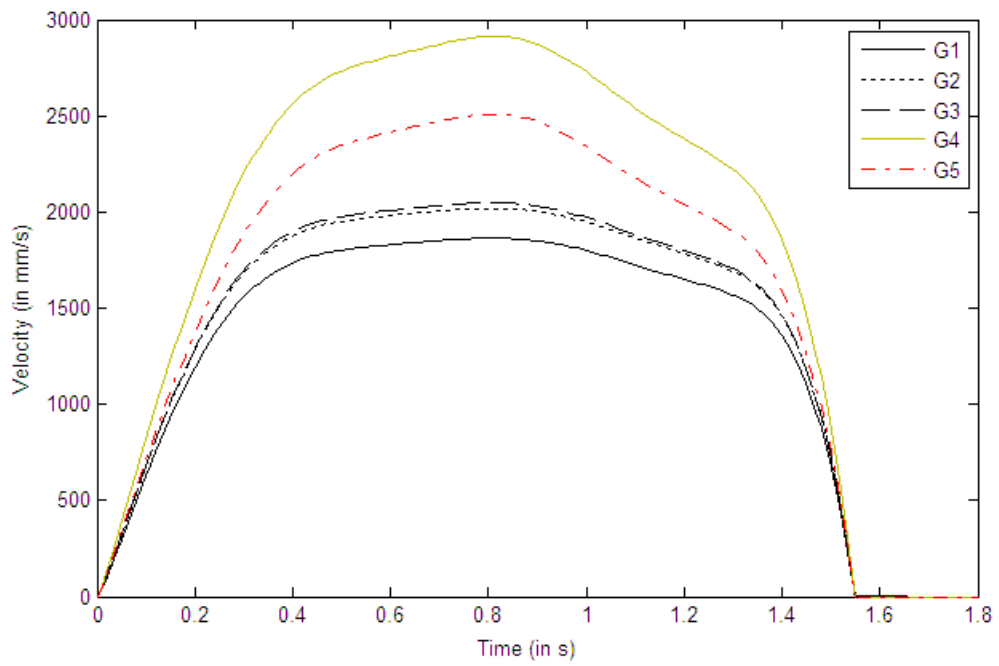


Figure 4.13 (c) – Velocity measurements across five generations (path 2)

# CHAPTER 5

## CONCLUSIONS, LIMITATIONS AND FUTURE WORK

### 5.1 CONCLUSIONS

The one-dimensional modelling of human lower airways has been done by using the Locally Conservative Galerkin (LCG) method. The method is demonstrated to handle geometric, material discontinuities and vessel branching. The geometric details published by Weibel and Horsfield was used to create the 1D network model of the airways. A realistic inflow measured at the Trachea has been used as the input to the network model. As a result, the flow variables viz., velocity, pressure and area have been calculated. It has been shown that the repetitive branching of the airways and the presence of geometric and material discontinuities gives rise to reflections which in turn affect the flow through the airways and in turn the regional ventilation of the lungs. This can be extended further to identify airway obstruction. The methodology presented has proved that some of the observable flow characteristic that cannot be measured in real life can be computed.

### 5.2 LIMITATIONS AND FUTURE WORK

The model assumes the flow to be laminar in the upper generations of the airways which is not physiological. In the future, the effects of turbulence shall be considered. Gravity can affect the regional ventilation of the lungs directly or by influencing the volume change by other organ movement. Its effect shall be studied in the future. It is very hard to find reliable information on the airway wall properties and effect of elongation of terminal bronchioles. These shall be studied in the future. Most importantly, changes in the cross-section at branching shall be considered. 3D models and hybrid coupled model shall be tried in the future as it is beyond the scope of this project.

# Bibliography

- 1 Allen, G.M., Shortall, B.P., Gemci, T., Corcoran, T.E., Chigier, N.A., 2004. Computational simulations of airflow in an in vitro model of the pediatric upper airways. *ASME Journal of Biomechanical Engineering* 126, 604-613.
- 2 Barnea, O., S. Abboud, et al. (1996). "New model-based indices for maximum expiratory flow-volume curve in patients with chronic obstructive pulmonary disease." *Computers in Biology and Medicine* 26(2): 123-131.
- 3 Bertram, C. D. (2008). "Flow-induced oscillation of collapsed tubes and airway structures." *Respiratory Physiology & Neurobiology* 163: 256–265.
- 4 Bijaoui, E., S. A. Tuck, et al. (1999). "Estimating respiratory mechanics in the presence of flow limitation." *J Appl Physiol* 86(Jan ): 418 - 426.
- 5 Bunk, D. A., W. J. Federspiel, et al. (1992). "Influence of Bifurcations on Forced Oscillations in an Airway Model." *Journal of Biomechanical Engineering* 114(2): 216-221.
- 6 Calay, R.K., Kurujareon, J., Holdø, A.E., 2002. Numerical simulation of respiratory flow patterns within the human lung. *Respiratory Physiology & Neurobiology* 130, 201-221.
- 7 Calay, R. K., J. Kurujareon, et al. (2002). "Numerical simulation of respiratory flow patterns within human lung." *Respiratory Physiology & Neurobiology* 130: 201–221
- 8 Cezbal, J.R., Summer, R.M., 2004. Tracheal and central bronchial aerodynamics using virtual bronchoscopy and computational fluid dynamics. *IEEE Transactions on Medical Imaging* 23(8), 1021-1023.
- 9 Comerford, A., C. A. Stahl, et al. (2008). Coupled 3D impedance model of the Human Lungs. *8th. World Congress on Computational Mechanics (WCCM8) and 5th European Congress on Computational Methods in Applied Sciences and Engineering (ECCOMAS 2008)*. Venice, Italy.
- 10 Dawson, C. A., G. S. Krenz, et al. (1999). "Structure-function relationships in the pulmonary arterial tree." *Journal of Applied Physiology* 86: 569-583.
- 11 De Backer, J. W., W. G. Vos, et al. (2007). "Flow analyses in the lower airways: Patient-specific model and boundary conditions." *Medical Engineering & Physics*.
- 12 Denny, E. and R. C. Schroter (1996). "A Mathematical Model for the Morphology of the Pulmonary Acinus." *Journal of Biomechanical Engineering* 118,: 210-215.
- 13 Denny, E. and R. C. Schroter (2006). "A model of non-uniform lung parenchyma distortion " *Journal of Biomechanics* 39(4): 652-663.
- 14 Du, Y. and A. M. Al-Jumaily (2006). "Obstruction identification in branching compliant tubes with application to airway passages." *Journal of Biomechanics* 39: 1363-1370.
- 15 Ernst, A., D. Feller-Kopman, et al. (2004). "Central Airway Obstruction - State of the art." *Am J of Respir Crit Care Med* 169.: 1278–1297.
- 16 Estépar, R. S. J., J. J. Reilly, et al. (2008). "Three-Dimensional Airway Measurements and Algorithms." *Proc Am Thorac Soc* 5: 905-909.
- 17 Evrensel, C. A., M. R. U. Khan, et al. (1993). "Viscous Airflow Through a Rigid Tube With a Compliant Lining: A Simple Model for the Air-Mucus Interaction in Pulmonary Airways." *J. Biomech. Eng.* 115: 262-270.

- 18 Farkas, Á. and I. Balásházy (2008). "Quantification of particle deposition in asymmetrical tracheobronchial model geometry." Computers in Biology and Medicine **38**(4): 508-518.
- 19 Fresconi, F. E. and A. K. Prasad (2007). "Convective dispersion during steady flow in the conducting airways of the human lung." Journal of Biomechanical Engineering **129** (5): 722-732.
- 20 Fresconi, F. E., A. S. Wexler, et al. (2008). "Transport profiles in the conducting airways of the human lung." International Journal of Heat and Mass Transfer **51**(23-24): 5552-5561
- 21 Freitas, R. K. and W. Schröder (2008). "Numerical investigation of the three-dimensional flow in a human lung model." Journal of Biomechanics **41**: 2446–2457.
- 22 Fung, Y. C., and S. S. Sobin. 1982. On the constitutive equation of the lung tissue. ASME Adv. Bioeng. 84-87.
- 23 Galvin, I., G. B. Drummond, et al. (2007). "Distribution of blood flow and ventilation in the lung: gravity is not the only factor." British Journal of Anaesthesia **98**(4): 420-8.
- 24 Gemci, T., V. Ponyavin, et al. (2008). "Computational model of airflow in upper 17 generations of human respiratory tract." Journal of Biomechanics **41**: 2047–2054.
- 25 Gemci, T., Corcoran, T.E., Chigier, N., 2002. A numerical and experimental study of spray dynamics in a simple throat-model. Aerosol Science and Technology 36(1), 18-38.
- 26 Gemci, T., Shortall, B., Allen, G., Corcoran, T.E., Chigier, N.A., 2003. CFD study of the throat during aerosol drug delivery using heliox and air. Journal of Aerosol Science 34, 1175-1192.
- 27 Grimal, Q., A. Watzky, et al. (2002)). "A one-dimensional model for the propagation of transient pressure waves through the lung." Journal of Biomechanics **35**: 1081–1089.
- 28 Guan, X., Martonen, T.B., 2000. Flow Transition in Bends and Applications to Airways. Journal of Aerosol Science 31(7), 833-847.
- 29 Hajji, M. A., T. A. Wilson, and S. J. Lai-Fook. 1979. Improved measurements of shear modulus and pleural membrane tension of the lung. J. Appl. Physiol. 47:175-181.
- 30 Horsfield, K., Dart, G., Olson, D.E., Filley, G.F., Cumming, G., 1971. Models of the human bronchial tree. Journal of Applied Physiology 31, 207-217.
- 31 Horsfield, K., W. I. Gordon, et al. (1987). "Growth of the bronchial tree in man." Thorax **42**: 383-388.
- 32 Horsfield, K., W. Kemp, et al. (1982). "An asymmetrical model of the airways of the dog lung." J. Appl. Physiol.: Respirat. Environ. Exercise Physiol. **52**(1): 21-26.
- 33 Hyatt, R.E., Wilcox, R.E., 1973. The pressure-flow relationship of the intrathoracic airways in man. J. Clin. Invest. 42, 29-39.
- 34 Kaye, S. R. and R. C. Schroter (1993). "An Experimental Model of Gas Dispersion and Uptake at the Bronchial Wall." Journal of Biomechanical Engineering **115**(1): 91-96.
- 35 Kitaoka, H., Takaki, R., Suki, B., 1999. A three-dimensional model of the human airway tree. Journal Applied Physiology 87(6), 2207-2217.
- 36 Kleinstreuer, C., Zhang, Z., 2003. Targeted drug aerosol deposition analysis for a four-generation pulmonary airway model with hemispherical tumors. ASME Journal of Biomechanical Engineering 125,197-206.
- 37 Kondo, T., I. Kobayashi, et al. (1998). "Contribution of airway resistance to airway pressure during mechanical ventilation: an experimental study." Tokai J Exp Clin Med **23**(1): 25-30.

- 38 Koombua, K. and R. M. Pidaparti (2008). "Inhalation Induced Stresses and Flow Characteristics in Human Airways through Fluid-Structure Interaction Analysis." Modelling and Simulation in Engineering **2008**,
- 39 Kriete, A., Schmidt, A.H., Zidowitz, S., Haworth, D.C., Kunz, R.F., 2004. Simulations at a newly derived reference model of the human lung. Proceedings of SPIE, Vol. 5318, pp. 163-169.
- 40 Lee, D.Y., Lee, J.W., 2002. Dispersion of aerosol bolus during one respiration cycle in a model of pulmonary airways. *Journal of Aerosol Science* 33, 1219-1234.
- 41 Liu, Y., So, R.M.C., Zhang, C.H., 2003. Modeling the bifurcating flow in an asymmetric human pulmonary airway. *Journal of Biomechanics* 36, 951-959.
- 42 Longest, P.W., Vinchurkar, S., 2007a. Effects of mesh style and grid convergence on particle deposition in bifurcating airway models with comparisons to experimental data. *Medical Engineering and Physics* 29(3), 350-366.
- 43 Longest, P. W., Vinchurkar, S., 2007b. Validating CFD predictions of respiratory aerosol deposition: effects of upstream transition and turbulence. *Journal of Biomechanics* 40, 305-316.
- 44 Longest, P.W., Vinchurkar, S., Martonen, T.B., 2006. Transport and deposition of respiratory aerosols in models of childhood asthma. *Journal of Aerosol Science* 37, 1234-1257.
- 45 Luo, H. Y. and Y. Liu (2008). "Modeling the bifurcating flow in a CT-scanned human lung airway." J. of Biomechanics.
- 46 Lu, D.-f., C. Stanley, et al. (1991). "A Mathematical Description of Pressures in Alveolar Pores of Kohn." Journal of Biomechanical Engineering **113**(1): 104-107.
- 47 Lutchen, K. R. and H. Gillis (1997). "Relationship between heterogeneous changes in airway morphometry and lung resistance and elastance." J. Appl. Physiol. **83**(4): 1192-1201.
- 48 Ma, B., Lutchen, K.R., 2006. An anatomically based hybrid computational model of the human lung and its application to low frequency oscillatory mechanics. *Annals of Biomedical Engineering* 34(11), 1691-1704.
- 49 Martonen, T. B., Y. Yang, et al. (1995). "Computer simulations of human lung structures for medical applications." Computers in Biology and Medicine **25**(5): 431-446.
- 50 Madasu, S., J. S. Ultman, et al. (2008). "Comparison of Axisymmetric and Three-Dimensional Models for Gas Uptake in a Single Bifurcation During Steady Expiration." Journal of Biomechanical Engineering **130**.
- 51 Madasu, S., J. S. Ultman, et al. (2006). "An Axisymmetric Single-Path Model for Gas Transport in the Conducting Airways." Journal of Biomechanical Engineering **128**: 69-75.
- 52 Mansour, K. F., J. A. Rowley, et al. (2002). "A mathematical model to detect inspiratory flow limitation during sleep." J Appl Physiol **93**(3): 1084-1092.
- 53 Mitchell, R. W., E. Ruhlmann, et al. (1997). "Conservation of bronchiolar wall area during constriction and dilation of human airways." J Appl Physiol **82**(3): 954-958.
- 54 Mols, G., V. Kessler, et al. (2001). "Is pulmonary resistance constant, within the range of tidal volume ventilation, in patients with ARDS?" British Journal of Anaesthesia **86**(2): 176-82.
- 55 Moskal, A. and L. Gradon (2002). "Temporal and spatial distribution of aerosol particles in the upper human airways during breathing cycles." J. Aerosol Sci. **33** 1525-1539.

- 56 Mynard, J.P. and P. Nithiarasu. (2008). A 1d arterial blood flow model incorporating ventricular pressure, aortic valve and regional coronary flow using the locally conservative galerkin (lcg) method. *Communications in Numerical Methods in Engineering*, 24:367-417.
- 57 Nithiarasu, P. (2004). A simple locally conservative galerkin (LCG) finite-element method for transient conse conservation equations. *Numerical Heat Transfer Part B - Fundamentals*, 46(4):357-370, 2004.
- 58 Nithiarasu, P.. A simple locally conservative galerkin (LCG) finite-element method for transient conservation equations. *Numerical Heat Transfer Part B - Fundamentals*, 46(4):357-370, 2004.
- 59 Nishida, M., Y. Inaba, et al. (1997). "Gas Dispersion in a Model Pulmonary Bifurcation During Oscillatory Flow." *Journal of Biomechanical Engineering* **119**(3): 309-316.
- 60 Nakayama, A., F. Kuwahara, et al. (2009). "Why do we have a bronchial tree with 23 levels of bifurcation?" *Heat mass transfer* **45**: 351-354.
- 61 Nowak, N., Kakade, P.P., Annapragada, A.V., (2003). "Computational fluid dynamics simulation of airflow and aerosol deposition in human lungs." *Annals of Biomedical Engineering* **31**,: 374–390.
- 62 Ochs, M., J. R. Nyengaard, et al. (2004). "The number of alveoli in the human lung." *American Journal of Respiratory and Critical Care Medicine* **169**: 120-124.
- 63 Palágyi, K., J. Tschirren, et al. (2006). "Quantitative analysis of pulmonary airway tree structures." *Computers in Biology and Medicine* **36**(9): 974-996
- 64 Pedley, T.J., Schroter, R.C., Sudlow, M.F., 1971. Flow and pressure drop in systems of repeatedly branching tubes. *Journal of Fluid Mechanics*, 46, 365-383.
- 65 Pedley, T.J., 1977. Pulmonary Fluid Dynamics. *Ann. Rev. Fluid Mech.* 9, 229-274.
- 66 Pedley, T. J., R. C. Schroter, et al. (1970). "Energy losses and pressure drop in models of human airways. ." *Respir Physiol* **9**: 371-386.
- 67 Pedley, T. J., R. C. Schroter, et al. (1971). "Flow and pressure drop in systems of repeatedly branching tubes." *Journal of Fluid Mechanics* **46**: 365-383.
- 68 Pedersen, O. F., H. J. L. Brackel, et al. (1997). "Wave-speed-determined flow limitation at peak flow in normal and asthmatic subjects." *J. Appl. Physiol.* **83**(5): 1721–1732.
- 69 Perlman, C. E. and J. Bhattacharya (2007). "Alveolar expansion imaged by optical sectioning microscopy." *J Appl Physiol* **103**(June): 1037–1044.
- 70 Polak, A. G. (1998). "A forward model for maximum expiration." *Computers in Biology and Medicine* **28**(6): 613-625.
- 71 Polak, A. G. and J. Mroczka (2006). "Nonlinear model for mechanical ventilation of human lungs." *Computers in Biology and Medicine* **36**(1): 41-58.
- 72 Pump, K. K. (1964). "The Morphology of the Finer Branches of the Bronchial Tree of the Human Lung." *Chest* **46**(4): 379-398.
- 73 Ratnovskya, A., D. Elad, et al. (2008). "Mechanics of respiratory muscles." *Respiratory Physiology & Neurobiology* **163**: 82–89.
- 74 Renotte, C., V. Bouffieux, et al. (2000). "Numerical 3D analysis of oscillatory flow in the time-varying laryngeal channel." *Journal of Biomechanics* **33**: 1637-1644.
- 75 Renotte, C., M. Remy, et al. (1998). "Dynamic model of airway pressure drop." *Med. Biol. Eng. Comput.* **36**: 101-106.

- 76 de Rochefort, L., L. Vial, et al. (2007). "In vitro validation of computational fluid dynamics simulation in human proximal airways with hyperpolarized  $^3\text{He}$  magnetic resonance phase-contrast velocimetry." J Appl Physiol **in press**.
- 77 Rozanek, M. and K. Roubik (2007). "Mathematical Model of the Respiratory System – Comparison of the Total Lung Impedance in the Adult and Neonatal Lung." Proceedings of World Academy of Science, Engineering and Technology **24**.
- 78 Rozanek, M. and K. Roubik "The Electric Circuit as a Model of the Human Respiratory System Matching to its Geometrical Proportions."
- 79 Sauret, V., P. M. Halson, et al. (2002). "Study of the three-dimensional geometry of the central conducting airways in man using computed tomographic (CT) images." J. Anat. **200**: 123–134.
- 80 Schmidt, A., Zidowitz, S., Kriete, A., Denhard, T., Krass, S., Peitgen, H.-O., 2004. A digital reference model of the human bronchial tree. Computerized Medical Imaging and Graphics **28**, 203-211.
- 81 Sera, T., Fujioka, H., Yokota, H., Makinouchi, A., Himeno, R., Schroter, R.C., Tanishita, K., 2003. Three-dimensional visualization and morphometry of small airways from microfocal X-ray computed tomography. Journal of Biomechanics **36**, 1587-1594.
- 82 Shi, H., Kleinstreuer, C., Zhang, Z., 2004. Nanoparticle transport and deposition in bifurcating tubes with different inlet conditions. Physics of Fluids **16**(7), 2199-2213.
- 83 Snyder, B., Dantzker, D.R., Jaeger, M.J., 1981. Flow partitioning in symmetric cascades of branches. Journal of Applied Physiology **51**(3), 598-506.
- 84 Spencer, R.M., Schroeter, J.D., Martonen, T.B., 2001. Computer simulations of pulmonary airway structures using data-driven surface modeling techniques. Computers in Biology and Medicine **31**, 499-511
- 85 Spencer, R. M., J. D. Schroeter, et al. (2001). "Computer simulations of lung airway structures using data-driven surface modeling techniques." Computers in Biology and Medicine **31**(6): 499-511.
- 86 Stapleton, K.W., Guentsch, E., Hoskinson, M.K., Finlay, W.H., 2000. On the suitability of k-epsilon modeling for aerosol deposition in the mouth and throat: A comparison with experiment. Journal of Aerosol Science **31**, 739-749.
- 87 Suki, B., and J. H. T. Bates. A nonlinear viscoelastic model of lung tissue mechanics. J. Appl. Physiol. **71**: 826–833, 1991.
- 88 Tawhai, M.H., Pullan, A.J., and Hunter, P.J., 2000. Generation of an anatomically based three-dimensional model of the conducting airways. Annals of Biomedical Engineering **28**, 793-802.
- 89 Tawhai, M. H., Hunter, P., Tschirren, J., Reinhardt, J., McLennan, G., Hoffman, E. A., 2004. CT-based geometry analysis and finite element models of the human and ovine bronchial tree. Journal Applied Physiology **97**(6), 2310-2321.
- 90 Tawhai, M. H., P. Hunter, et al. (2004). "CT-based geometry analysis and finite element models of the human and ovine bronchial tree." Journal Applied Physiology **97**(6): 2310–2321.
- 91 Teng, Z., I. Ochoa, et al. (2008). "Study of tracheal collapsibility, compliance and stress by considering its asymmetric geometry." Medical Engineering & Physics.
- 92 Tgavalekos, N.T., Venegas, J.G., Suki, B., Lutchen, K.R., 2003. Relation between structure, function, and imaging in a three-dimensional model of the lung. Annals of Biomedical Engineering **31**, 363-373.
- 93 Thomas, C.G. and P. Nithiarasu, R.L.T. Bevan, The locally conservative Galerkin (LCG) method for incompressible Navier-Stokes equations, International Journal for Numerical Methods in Fluids, **57**, 1771-1792, 2008.



- 94 Thomas, C.G. and P. Nithiarasu. An element-wise, locally conservative galerkin (LCG) method for solving diffusion and convection-diffusion problems. *International Journal for Numerical Methods in Engineering*, In Press, 2007.
- 95 Thomas, C.G.. A locally conservative Galerkin (LCG) finite element method for convection-diffusion and Navier-Stokes equations. PhD thesis, University of Wales Swansea, 2006.
- 96 C.G. Thomas. A locally conservative Galerkin (LCG) finite element method for convection-diffusion and Navier-Stokes equations. PhD thesis, University of Wales Swansea, 2006.
- 97 van Ertbruggen, C., Hirsch, C, Paiva, M., 2005. Anatomically based three-dimensional model of airways to simulate flow and particle transport using computational fluid dynamics. *Journal of Applied Physiology* 98(3), 970-980.
- 98 Weibel, E.R., 1963. *Morphometry of the Human Lung*, Springer Verlag, Berlin.
- 99 West, J. B. and C. T. Dollery (1965). "Distribution of blood flow and the pressure-flow relations of the whole lung." *J Appl Physiol* 20(2): 175-183.
- 100 West JB, *Respiratory Physiology, The Essentials*, 6<sup>th</sup> ed. 2000, Lippincott, p. 95.
- 101 Weibel, E. R. (1963). "Morphometry of the human lung." *Science*: 115-126.
- 102 Wiechert, L. and W. A. Wall (2008). Multi-Scale Analysis of Coupled Lung Tissue Dynamics. 8th. World Congress on Computational Mechanics (WCCM8) and 5th European Congress on Computational Methods in Applied Sciences and Engineering (ECCOMAS 2008). Venice, Italy.
- 103 Wilson, T. A. (1978). "Modeling the effect of axial bronchial tension on expiratory flow." *J Appl Physiol* 45(5): 659-665.
- 104 Wilquem, F. and G. Degrez (1997). "Numerical modeling of steady inspiratory airflow through a three-generation model of the human central airways." *J Biomech Eng* 119: 59-65.
- 105 [www.wikipedia.org](http://www.wikipedia.org)
- 106 Yang, X. L., Y. Liu, et al. (2006). "Respiratory flow in obstructed airways." *J. Biomech. Eng.* 39: 2743-2751.
- 107 Yang, X., Y. Liu, et al. (2006). "The effect of inlet velocity profile on the bifurcation COPD airway flow." *Comput Biol Med* 36: 181-194.
- 108 Yeh H. C. and S. GM. (1980). "Models of the human lung airways and their application to inhaled particle deposition." *Bull Math Biol* 42: 461-480.
- 109 Yeates, D. B. and N. Aspin (1978). "A mathematical description of the airways of the human lung." *Respiration Physiology*, 32: 91-104.
- 110 Zhang, Z and Kleinstreuer, C., 2004. Airflow structures and nano-particle deposition in a human upper airway model. *Journal of Computational Physics* 198, 178-210.
- 111 Zhang, Z., Kleinstreuer, C., Kim, C.S., 2002. Cyclic Micron-size Particle Inhalation and Deposition in a Triple Bifurcation Lung Airway Model. *Journal of Aerosol Science* 33, 257-281.
- 112 Zhao, Y., Lieber, B.B., 1994. Steady inspiratory flow in a model symmetric bifurcation. *ASME Journal of Biomechanical Engineering* 116, 488-496.
- 113 Zhao, Y., Lieber, B.B., (1994b). "Steady expiratory flow in a model symmetric bifurcation." *Journal of Biomechanical Engineering* 116,; 318-323.

- 114 Zheng, Y., J. C. Anderson, et al. (2005). "Effect of Gravity on Liquid Plug Transport Through an Airway Bifurcation Model." Journal of Biomechanical Engineering **127**(5): 798-806.